13.0 APPENDIX B. UPWARD FLOW TANK DIMENSIONS AND APPARATUS

The sedimentation tank was made from perspex with an inner diameter of 895mm and a depth of 400mm. The floor slope is 60° so that hydrostatic de-sludging is possible.

The feed pipe enters the side of the tank and turns through 90° when it reaches the centre and terminates in a bellmouth. It discharges in a vertical direction a short distance below the water level. Around the feed pipe is a stilling box, 150mm in diameter and extends a little to the bottom of the vertical walls. This produces an effective settling area of 0,612m². V-notch weirs direct the effluent into the effluent launders (see photographs below).

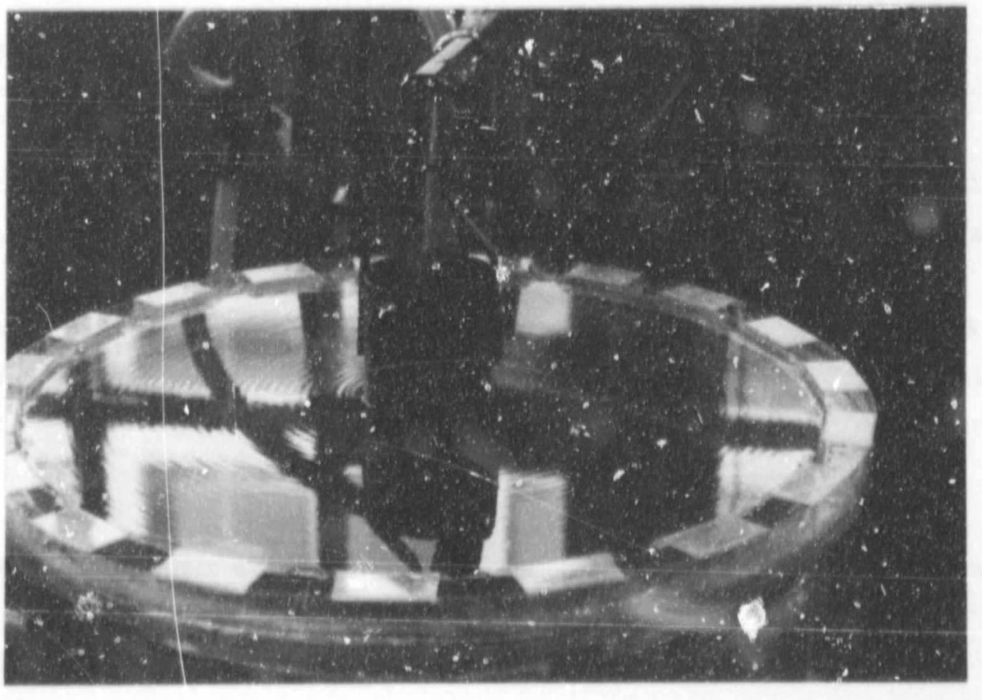

Figure 91. Effluent launder arrangement of upward flow settler.

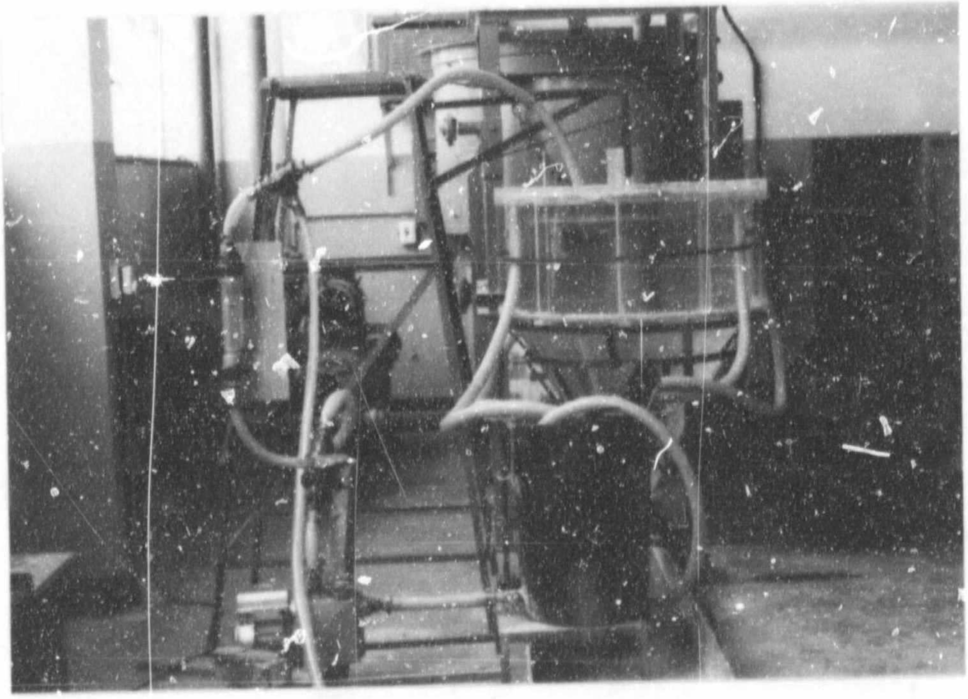

Figure 92. Upward flow tank and apparatus.

The upward flow tank was operated on a closed circuit system. The influent was mixed in a 70 litre bucket which was continuously stirred by means of a mechanical stirrer. The influent was then pumped into the sedimentation tank with a flow meter situated in between. The tank was desludged continuously at a constant rate of 0,45m^3/h. Sludge and effluent were then returned into the bucket to complete the loop (see figure 93 below and photograph above).

The same dehydrated mine sludge that was used in the batch settling tests was used to obtain various feed concentrations. The system was run for 1 to 1½ hours at different overflow rates before samples of the influent, effluent and sludge were taken. This was done to allow the system to reach equilibrium for a specific overflow rate. The samples were then tested for SS concentrations (see APPENDIX J for method).

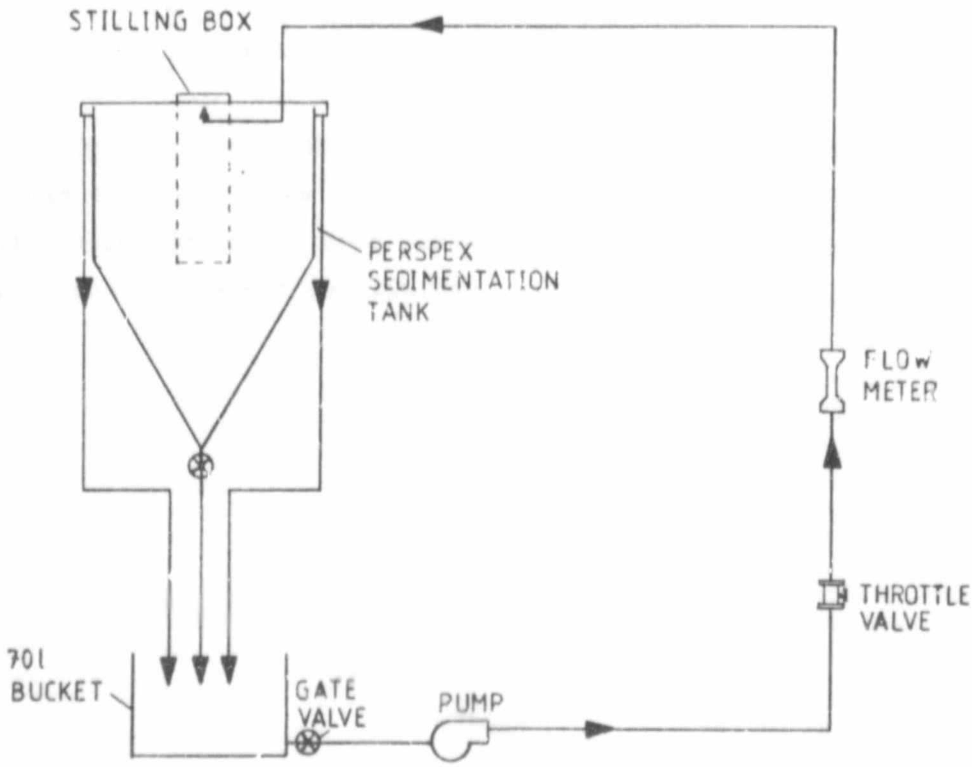

Figure 93. Flow network of upward flow tank.

The temperature of the water in the tank was recorded regularly and the overflow rate was adjusted to obtain results at a uniform temperature of 20°C. In this way the effect of varying sedimentation efficiencies due to the change of the kinematic viscosity ν with temperature was excluded. Values used in adjusting the overflow rates were:

TEMP °C	10	15	20	25	30
$\nu \times 10^{-6} m^2/s$	1,31	1,15	1,01	0,9	0,8

Since the relationship between overflow rate v and kinematic viscosity ν is linear in settling theory, the adjusted overflow rate at a temperature of 20°C was obtained as follows:

$$v_T = v_{20} \times (1,01/\nu_T)$$

where v_{20} - overflow rate at 20°C

v_T - overflow rate at recorded temperature

ν_T - kinematic viscosity at recorded temperature

The overflow rate was adjusted by either opening or closing the throttle valve. Six overflow rates (v_{20}) were used (0,6; 1,6; 2,6; 3,6; 4,6; 5,6m/h). Values for $v > 5{,}6$m/h could not be used since the measuring capacity of the flow meter was limited.

14.0 APPENDIX C. UPWARD FLOW TANK RESULTS AND BATCH SETTLING DATA

The results of the upward flow tank tests were plotted on graphs of influent SS concentration in mg/l vs the percent suspended solids removal. This was done for the six overflow rates mentioned in APPENDIX B, all at a constant temperature. On the same graph the predicted performance of the sedimentation tank obtained from the batch settling tests was plotted. These results were once again adjusted to a temperature of 20°C via the kinematic viscosity as shown in APPENDIX B.

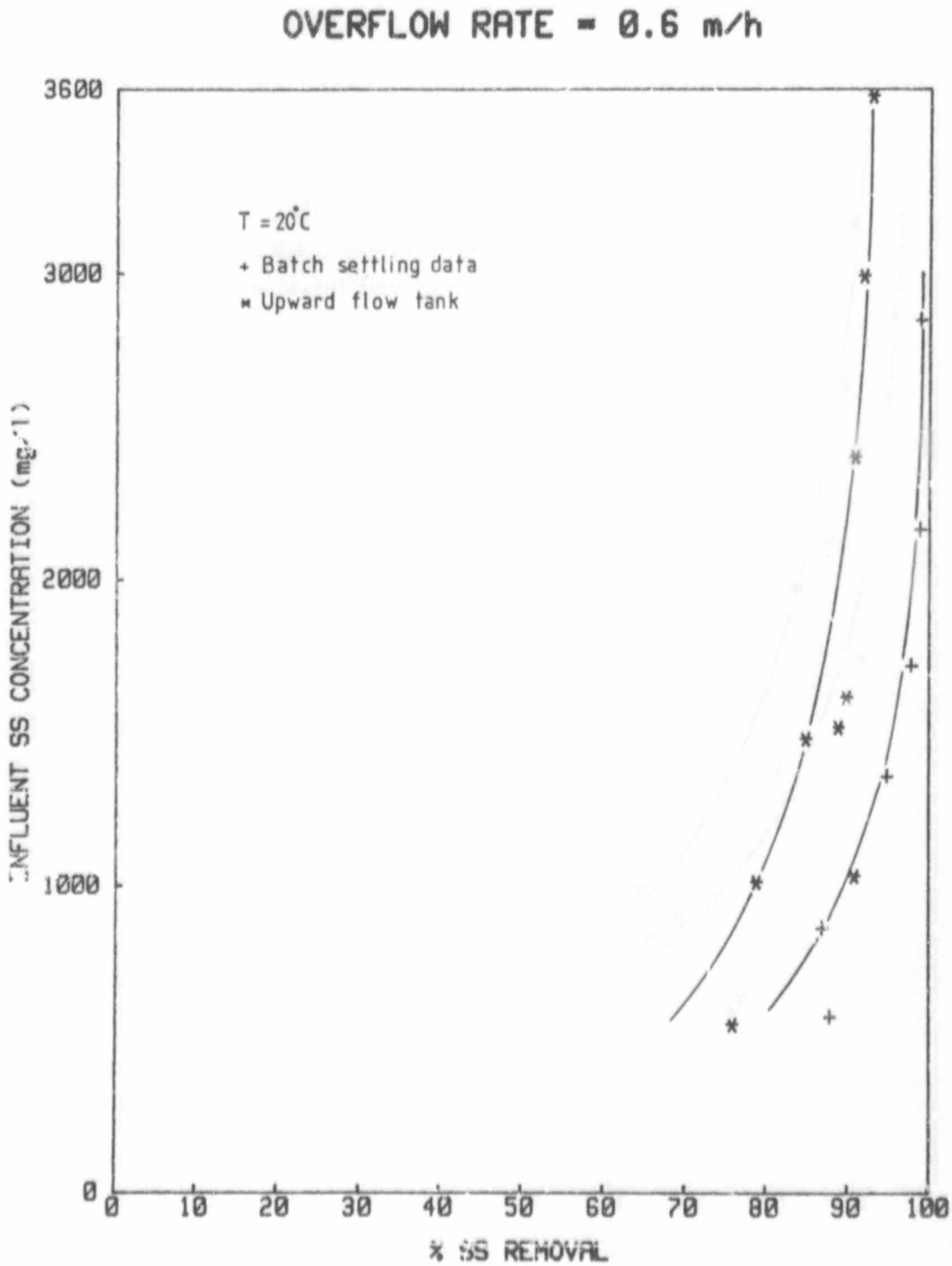

Figure 94. Influent SS concentration vs % SS Removal. Overflow rate = 0,6m/h.

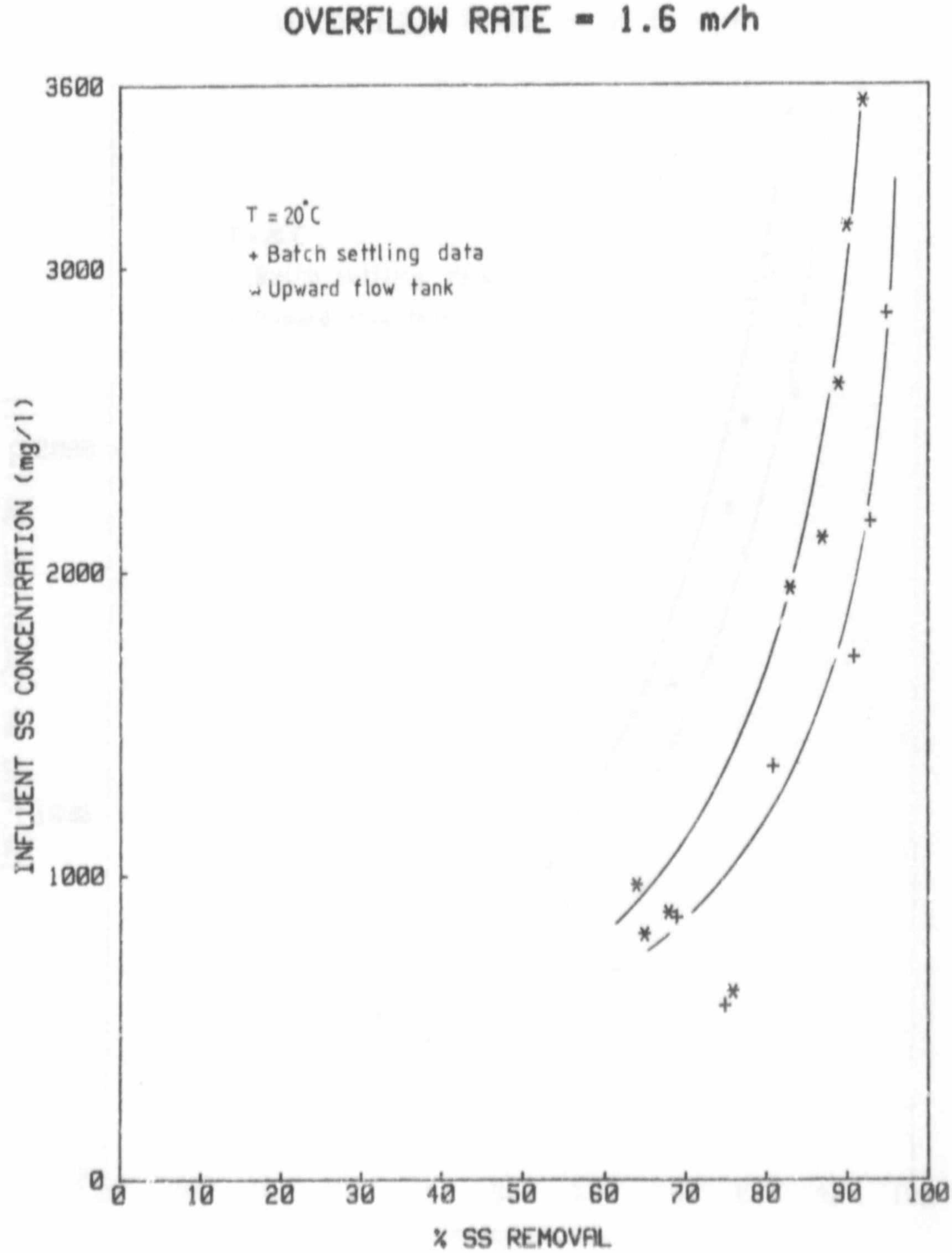

Figure 95. Influent SS concentration vs % SS Removal. Overflow rate = 1,6m/h.

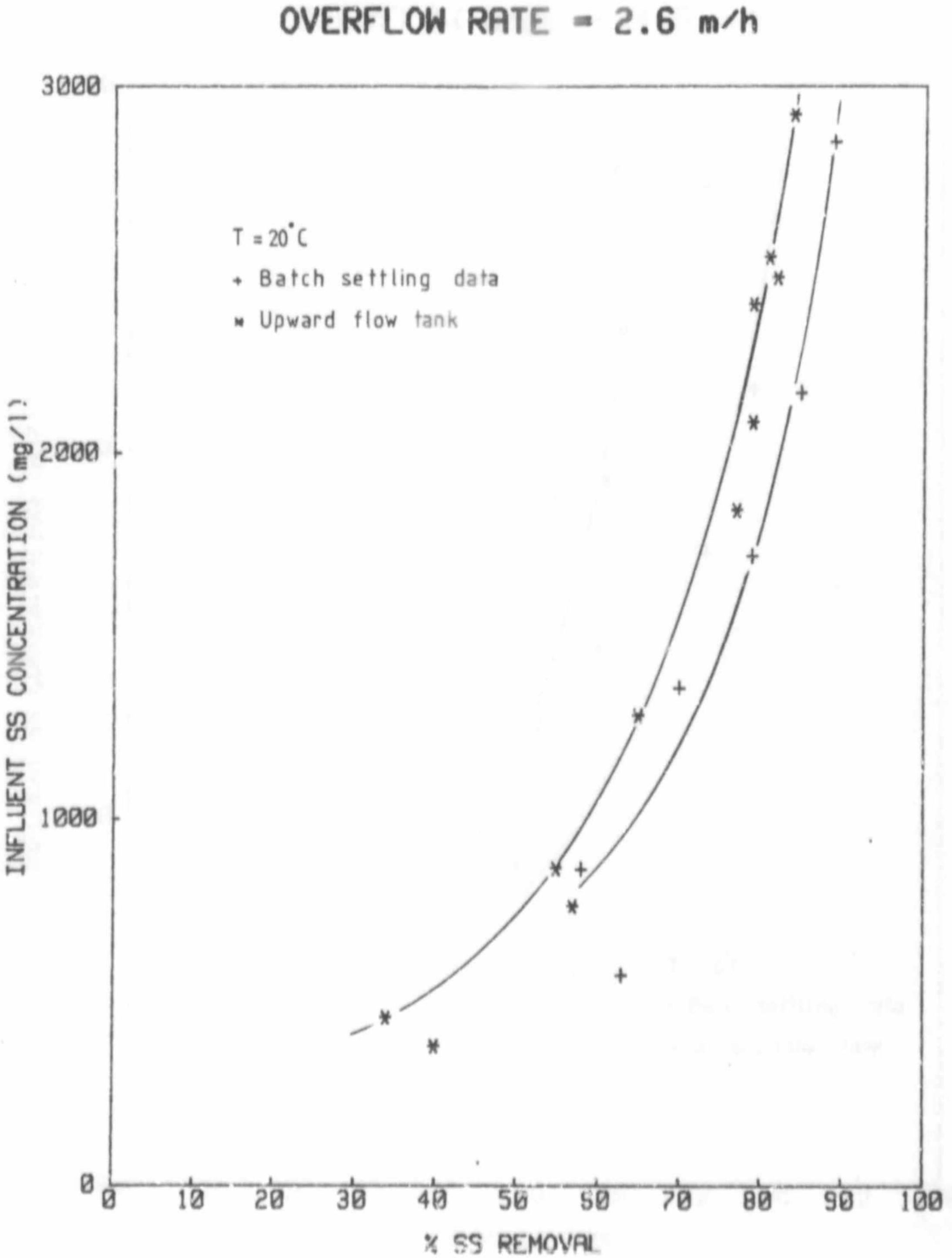

Figure 96. Influent SS concentration vs % SS Removal. Overflow rate = 2,6m/h.

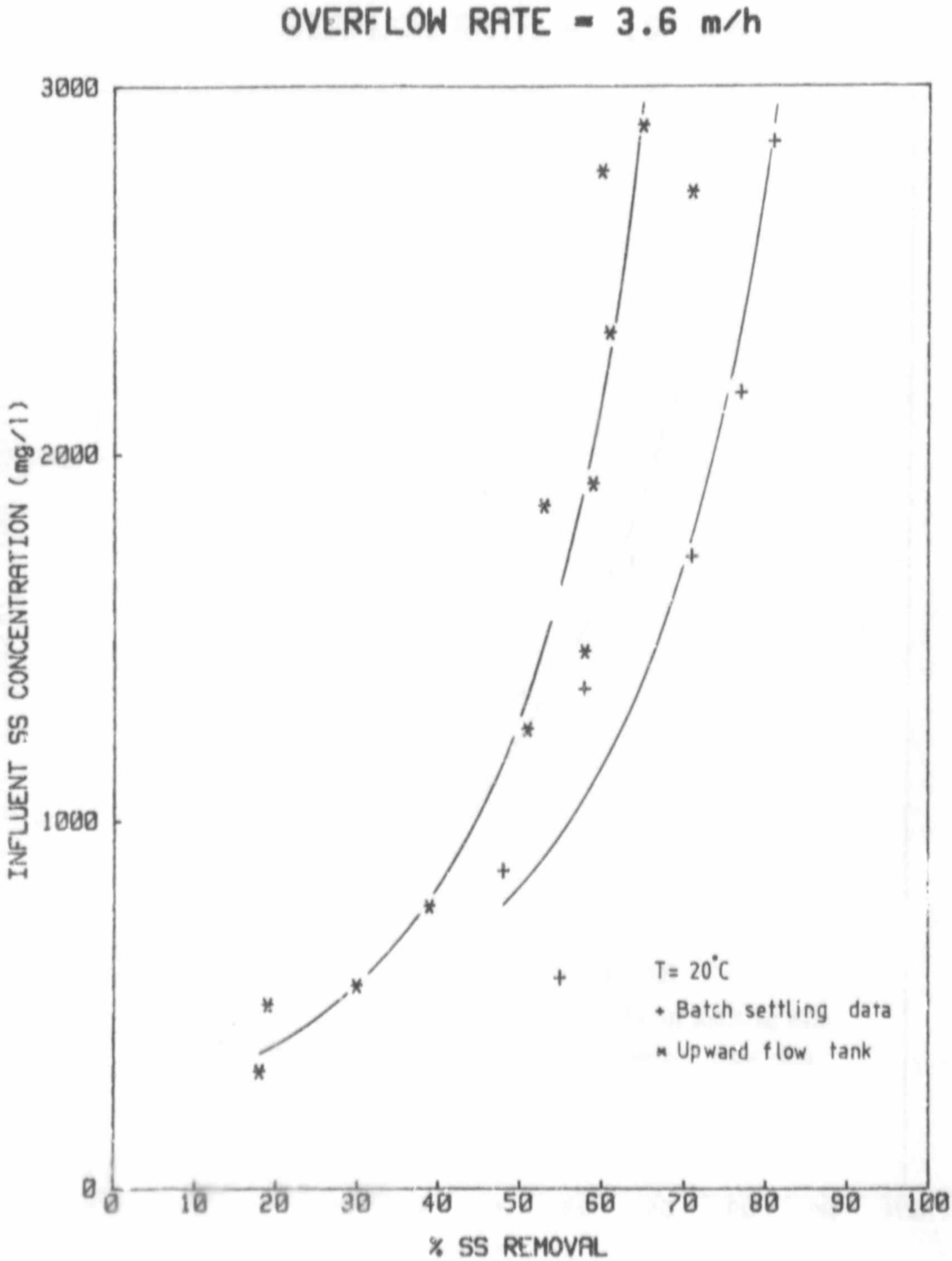

Figure 97. Influent SS concentration vs % SS Removal. Overflow rate = 3,6m/h.

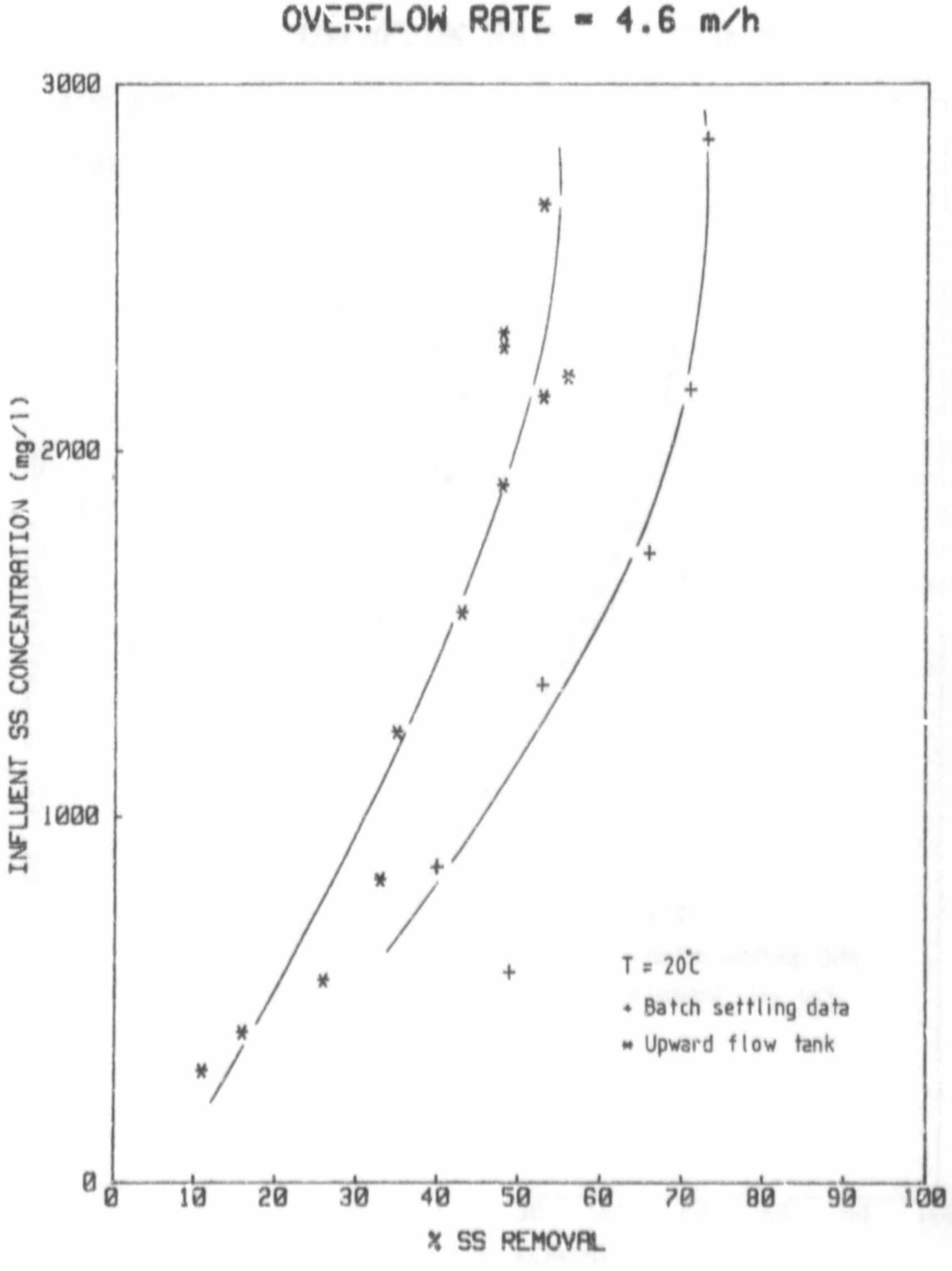

Figure 98. Influent SS concentration vs % SS Removal. Overflow rate = 4,6m/h.

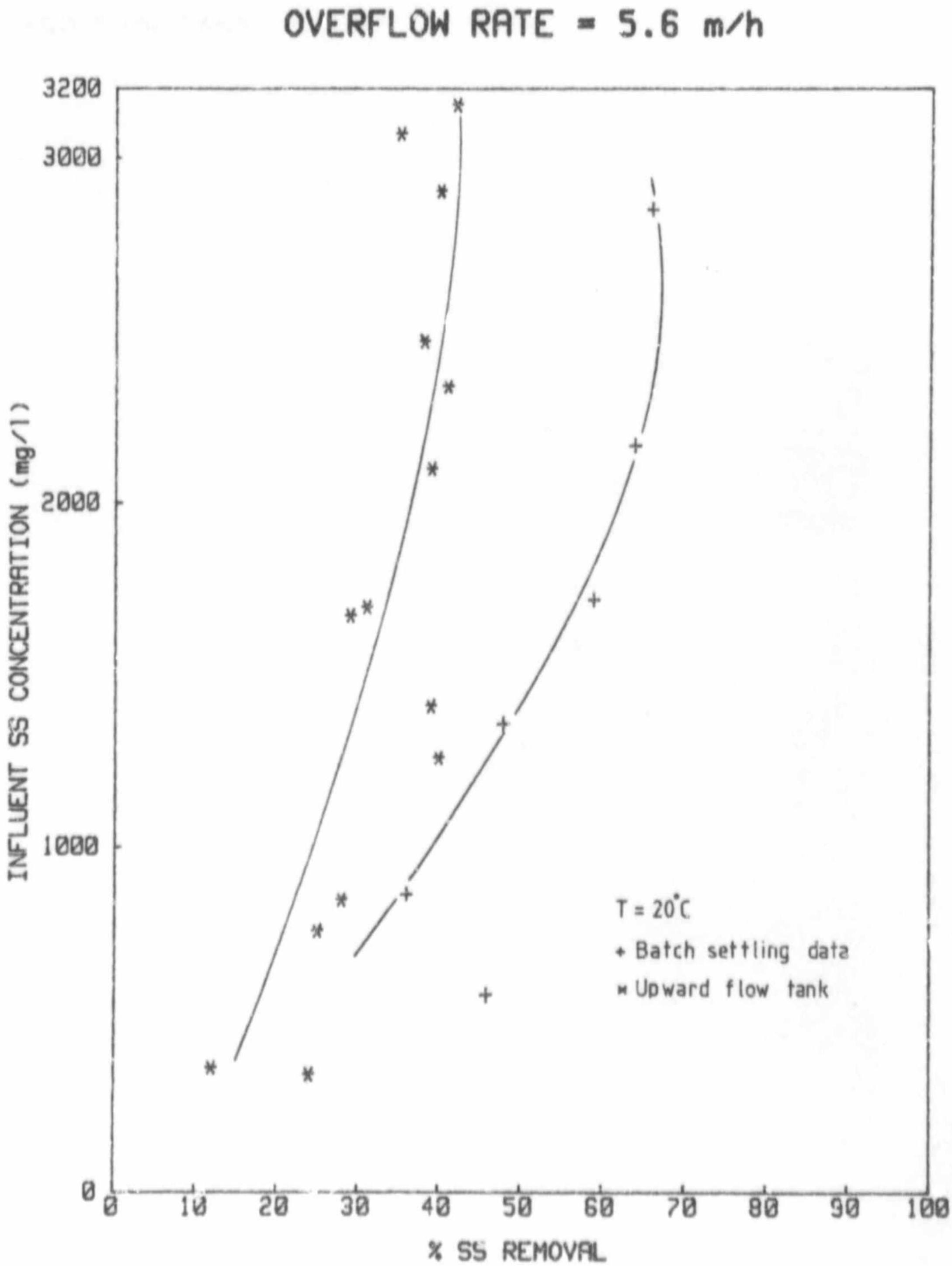

Figure 99. Influent SS concentration vs % SS Removal. Overflow rate = 5,6m/h.

15.0 APPENDIX D. POTASSIUM PERMANGANATE TRACER IN THE UPWARD FLOW TANK

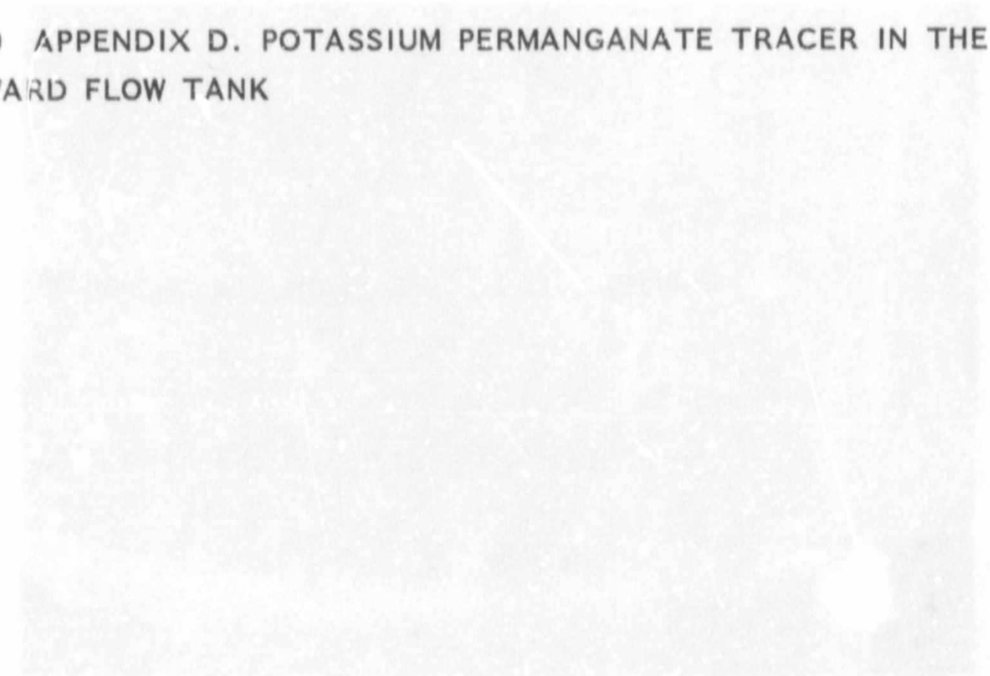

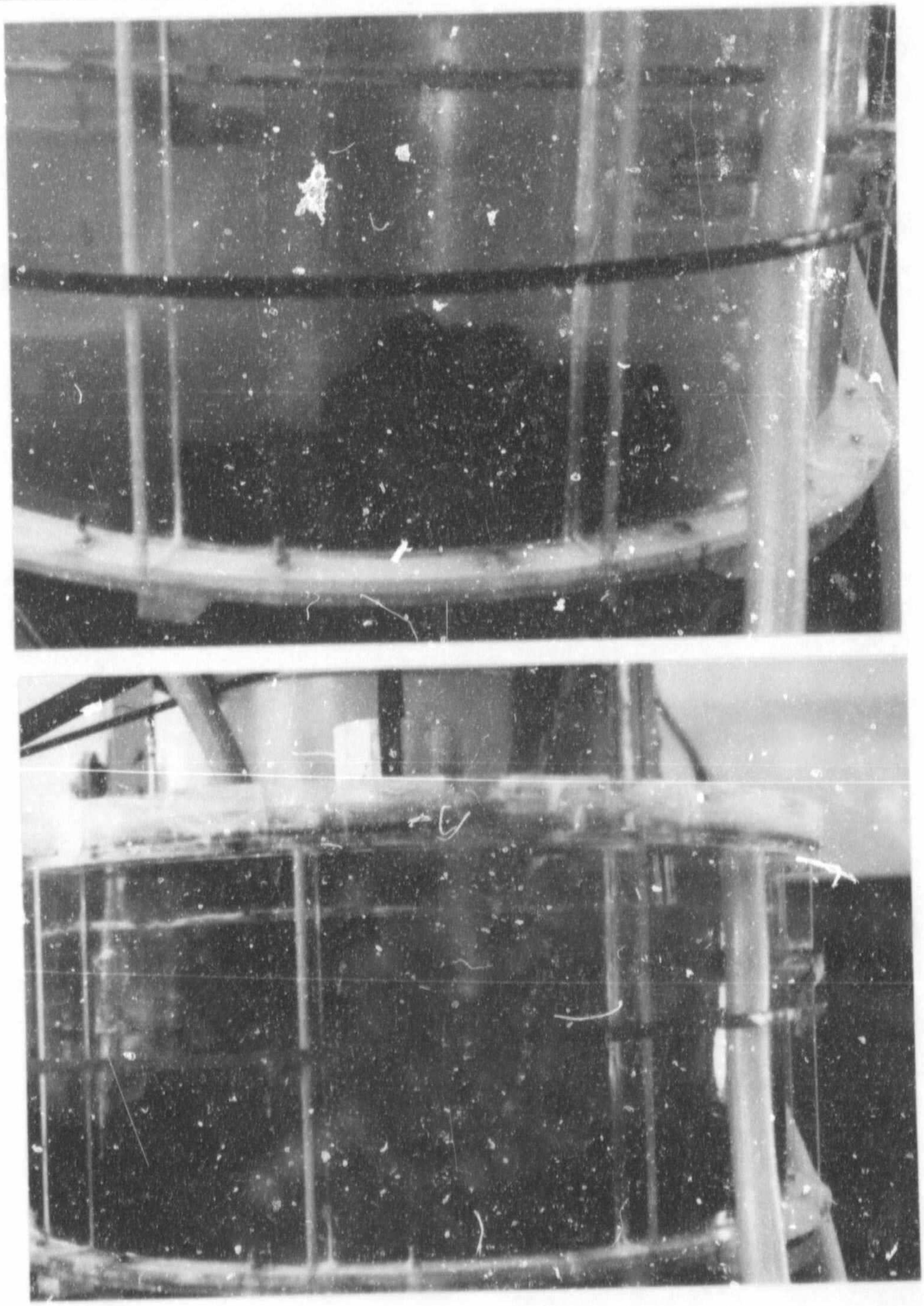

Figure 100. Photographs showing turbulent flow patterns in the upward flow tank.: The photographs clearly show that ideal plug flow conditions are non-existant in a conventional upward flow clarifier.

16.0 APPENDIX E. WORKING DRAWINGS OF CONICAL LAMELLA MODEL.

This APPENDIX gives the working drawings of the cones that were constructed and installed within the perspex sedimentation model tank.

SETTLING CONE

FRONT ELEVATION

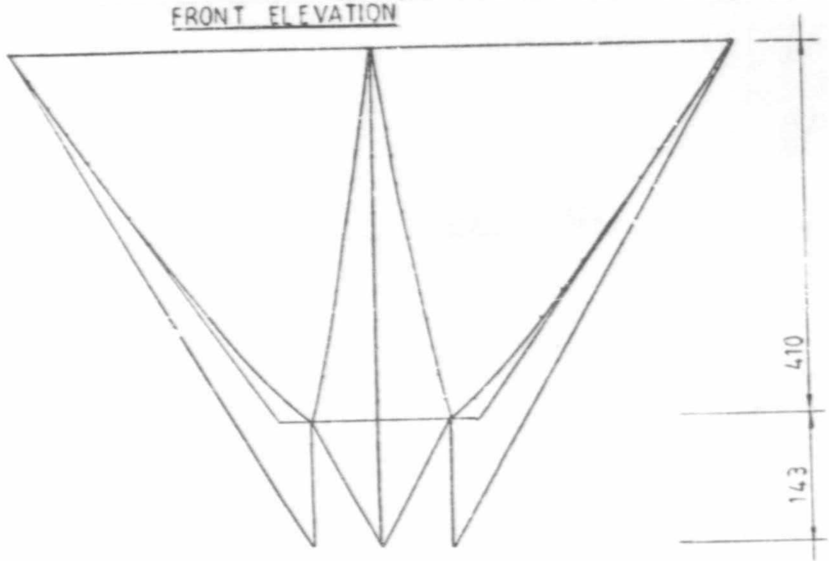

PLAN

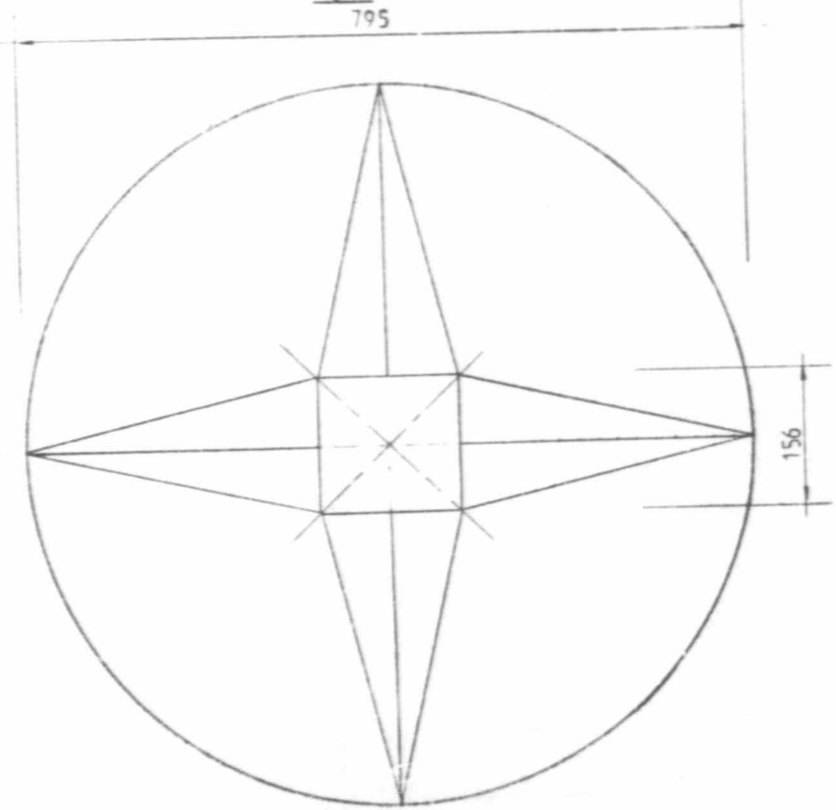

TRUE SHAPE OF TRIANGULAR GUTTER

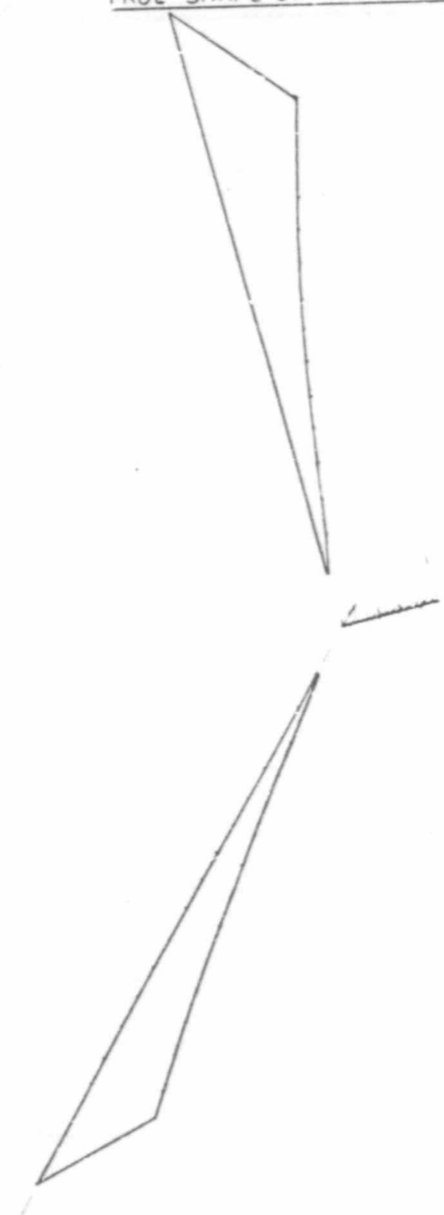

Scale 1:6

CONE LAMELLA SETTLER

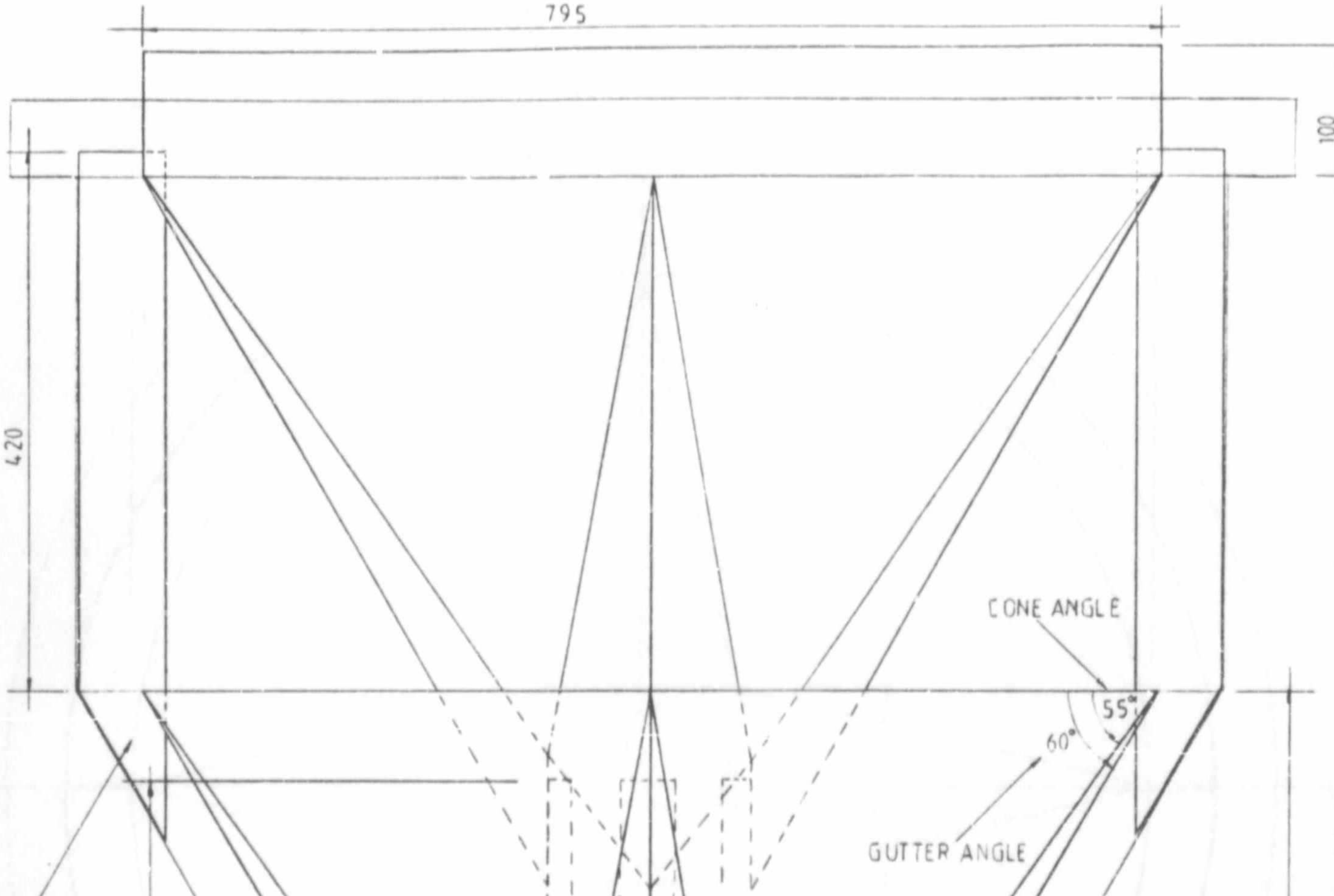

Scale 1:4
6 CONES INCLUDING TOP ONE

PLAN OF CONE LAMELLA

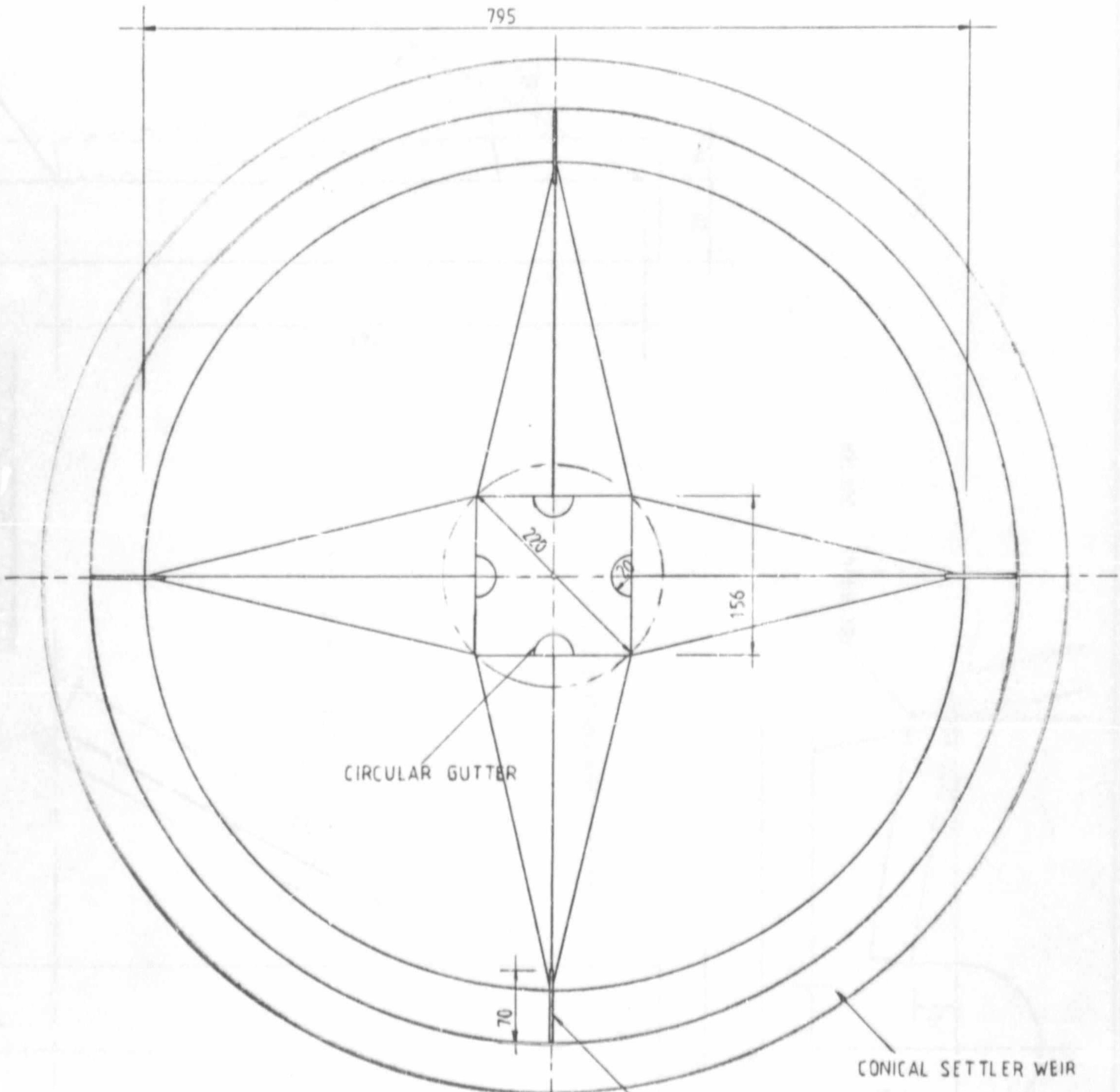

Scale 1:4

GUTTER ARRANGEMENT

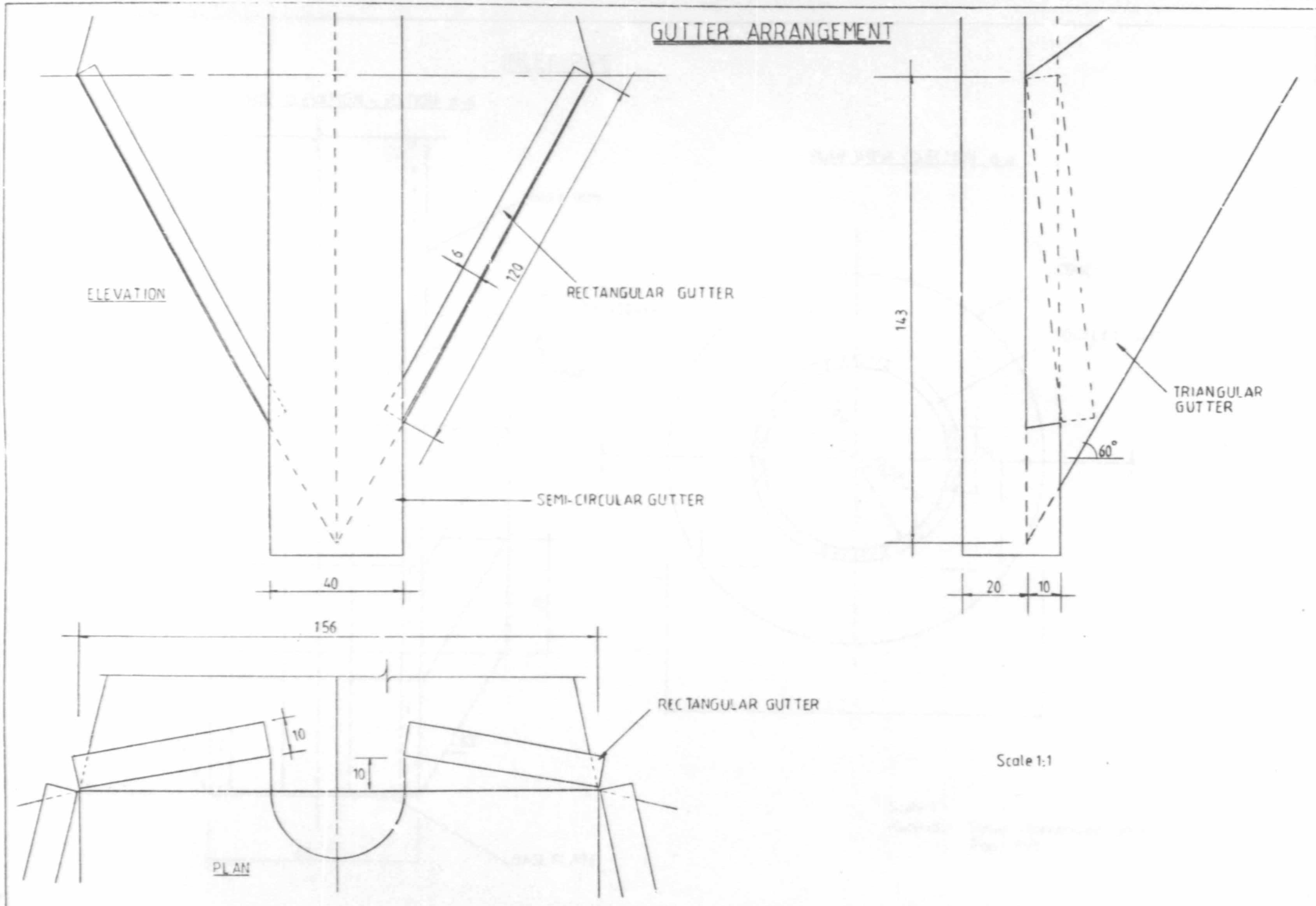

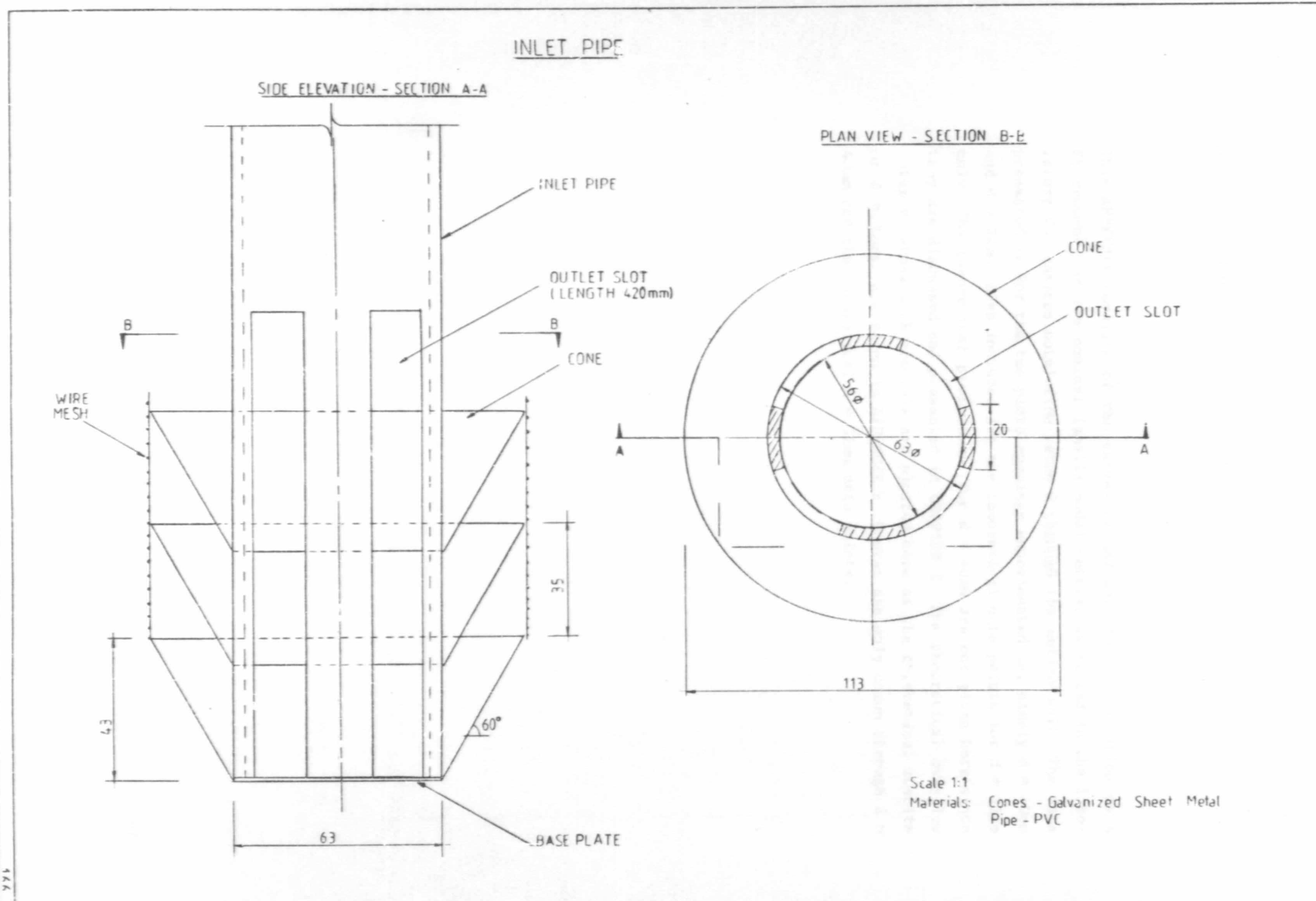
INLET PIPE
SIDE ELEVATION - SECTION A-A
INLET PIPE
OUTLET SLOT
(LENGTH 420mm)
B
B
CONE
WIRE MESH
35
43
60°
63
BASE PLATE
PLAN VIEW - SECTION B-B
CONE
OUTLET SLOT
56ø
20
63ø
A
A
113
Scale 1:1
Materials: Cones - Galvanized Sheet Metal
Pipe - PVC

17.0 APPENDIX F. CONICAL LAMELLA PERFORMANCE RESULTS.

This APPENDIX consists of the curves of influent SS concentration vs % SS removed for the conical lamella model settler as tested in the laboratory for various total flow rates Q through the entire unit. The data presented is for the two plate spacings experimented on, namely d = 40mm and d = 32mm. Also included are the theoretical data points for d = 32mm only. The theoretical predictions for d = 40mm are not given here since they are discussed and presented in CHAPTER 8. The theoretical overflow rates v whose % SS removals are plotted here as the theoretical results of d = 32mm, are given in APPENDIX H. Curves are only drawn through d = 40mm and the theoretical d = 32mm data points.

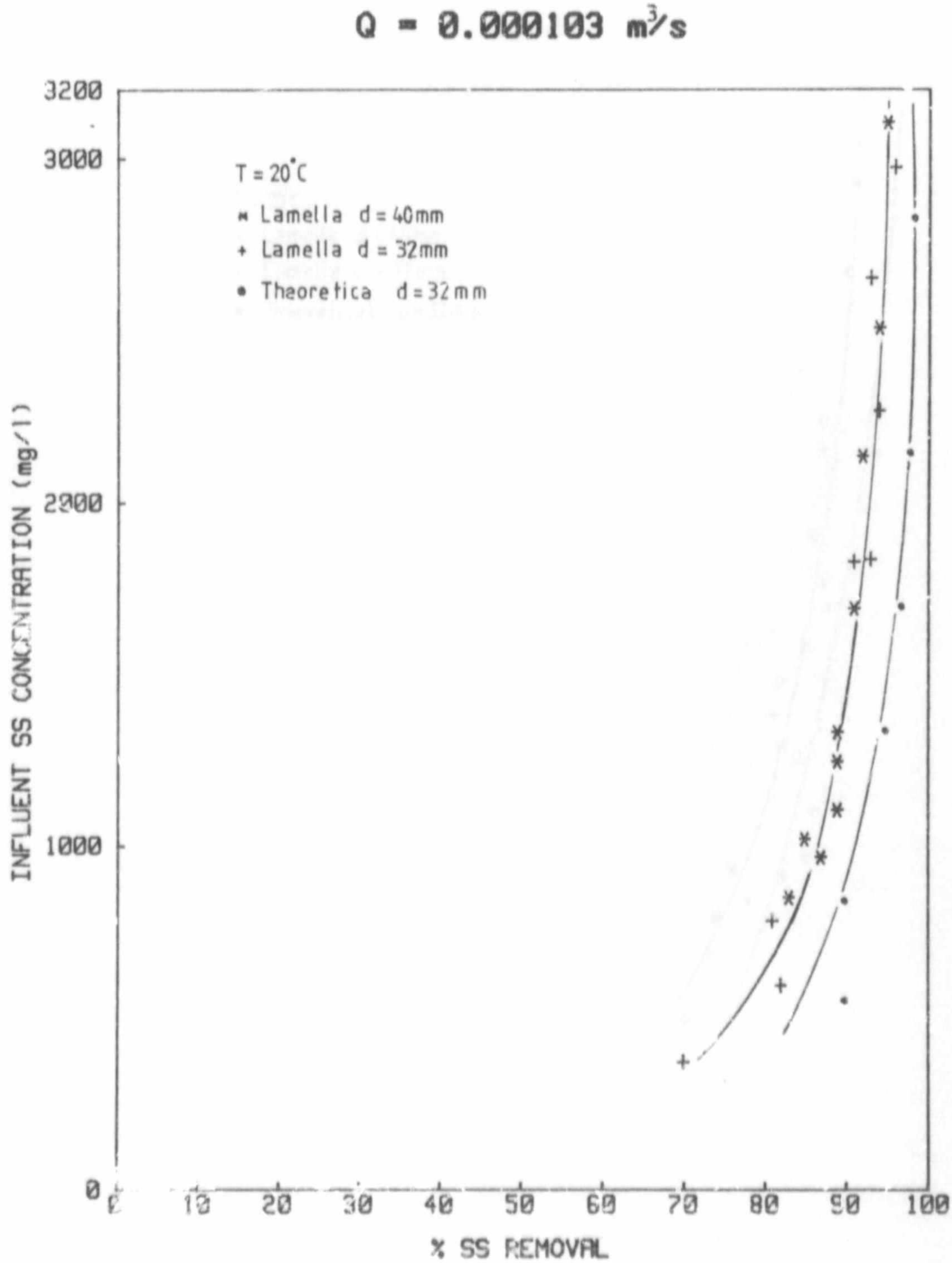

Figure 101. Influent SS concentration vs % SS removal. Q = 0,000103m³/s.

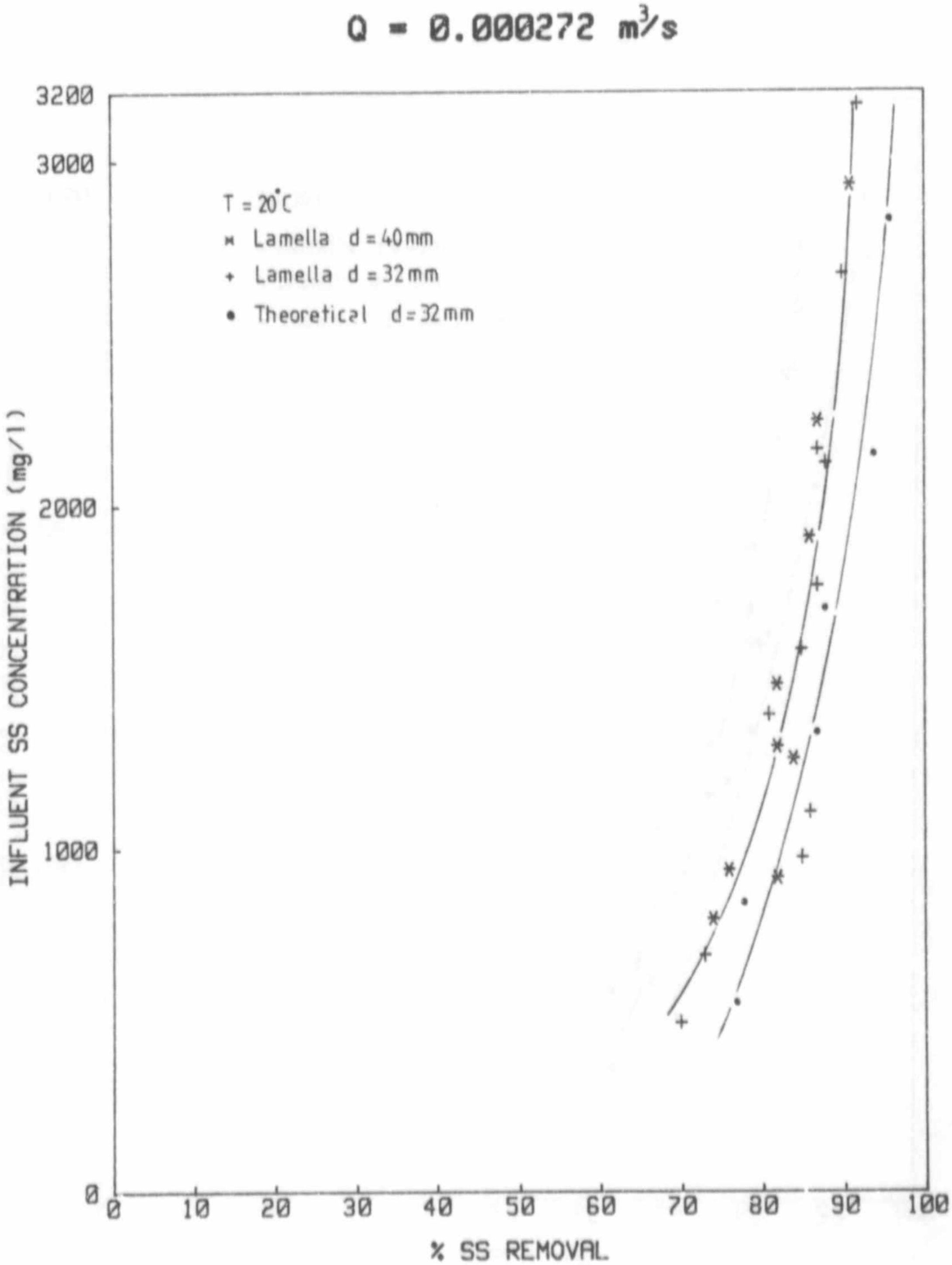

Figure 102. Influent SS concentration vs % SS removal. Q = 0,000272m³/s.

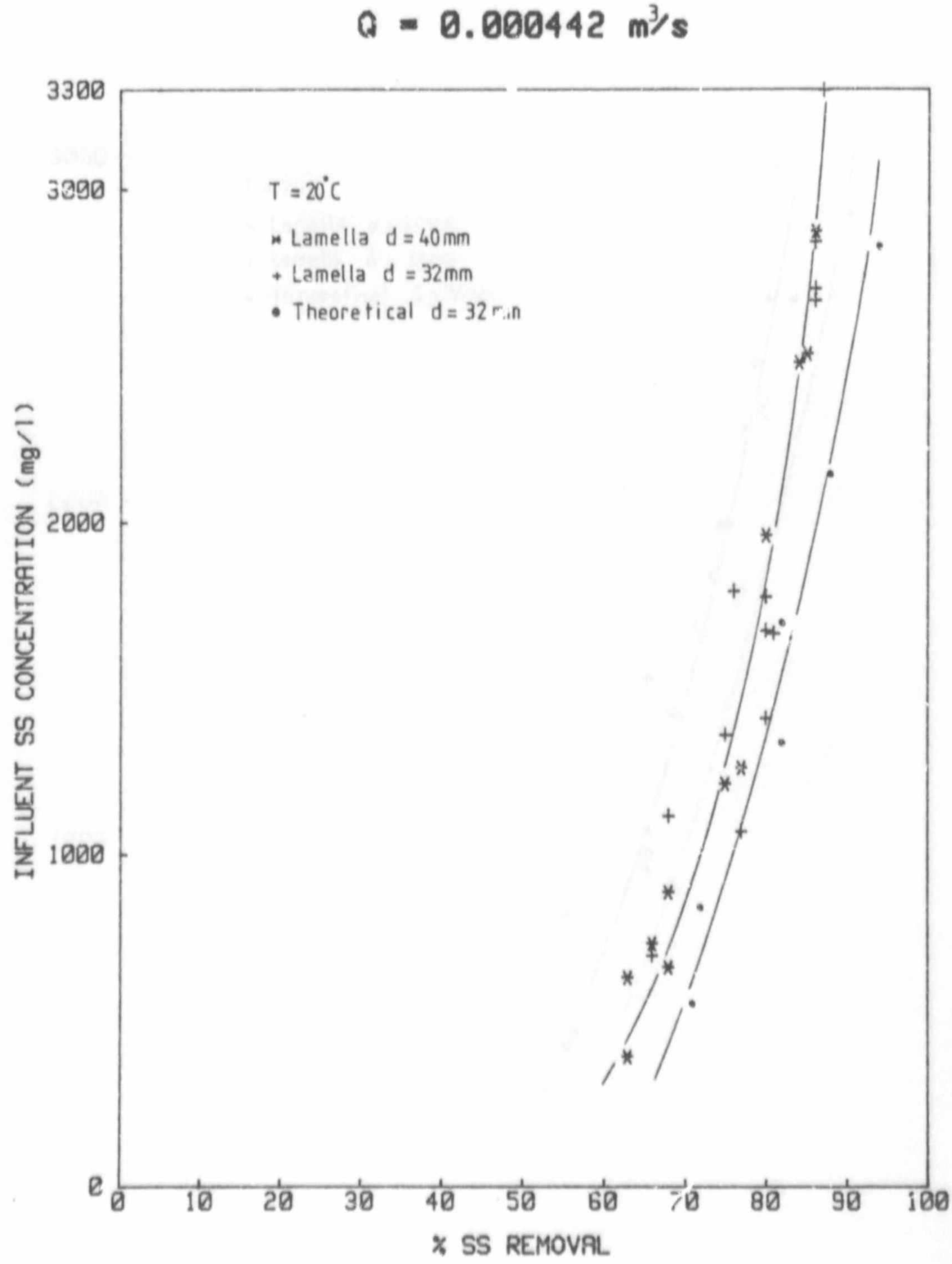

Figure 103. Influent SS concentration vs % SS removal. Q = 0,000442m³/s.

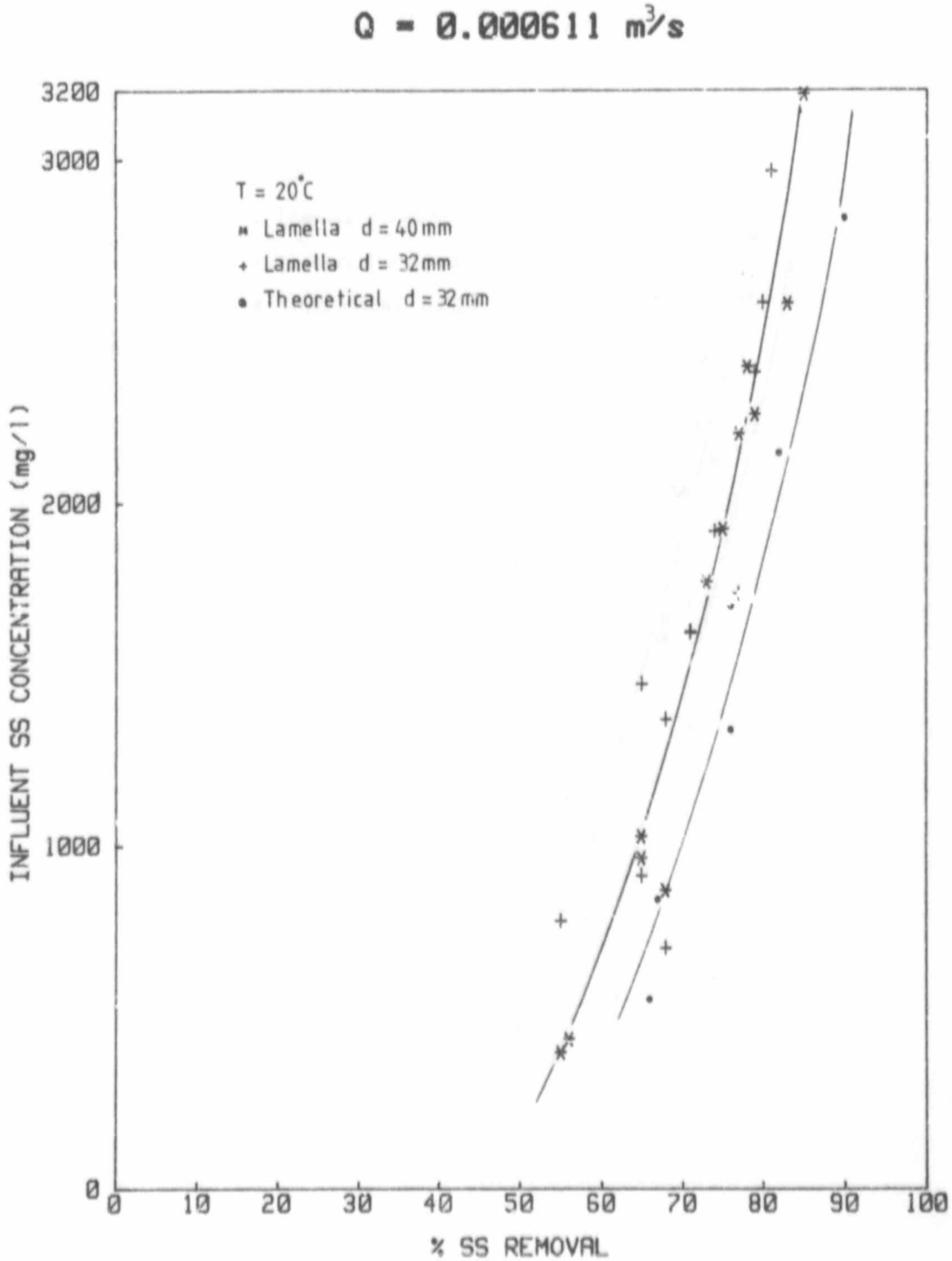

Figure 104. Influent SS concentration vs % SS removal. Q = 0,000611m³/s.

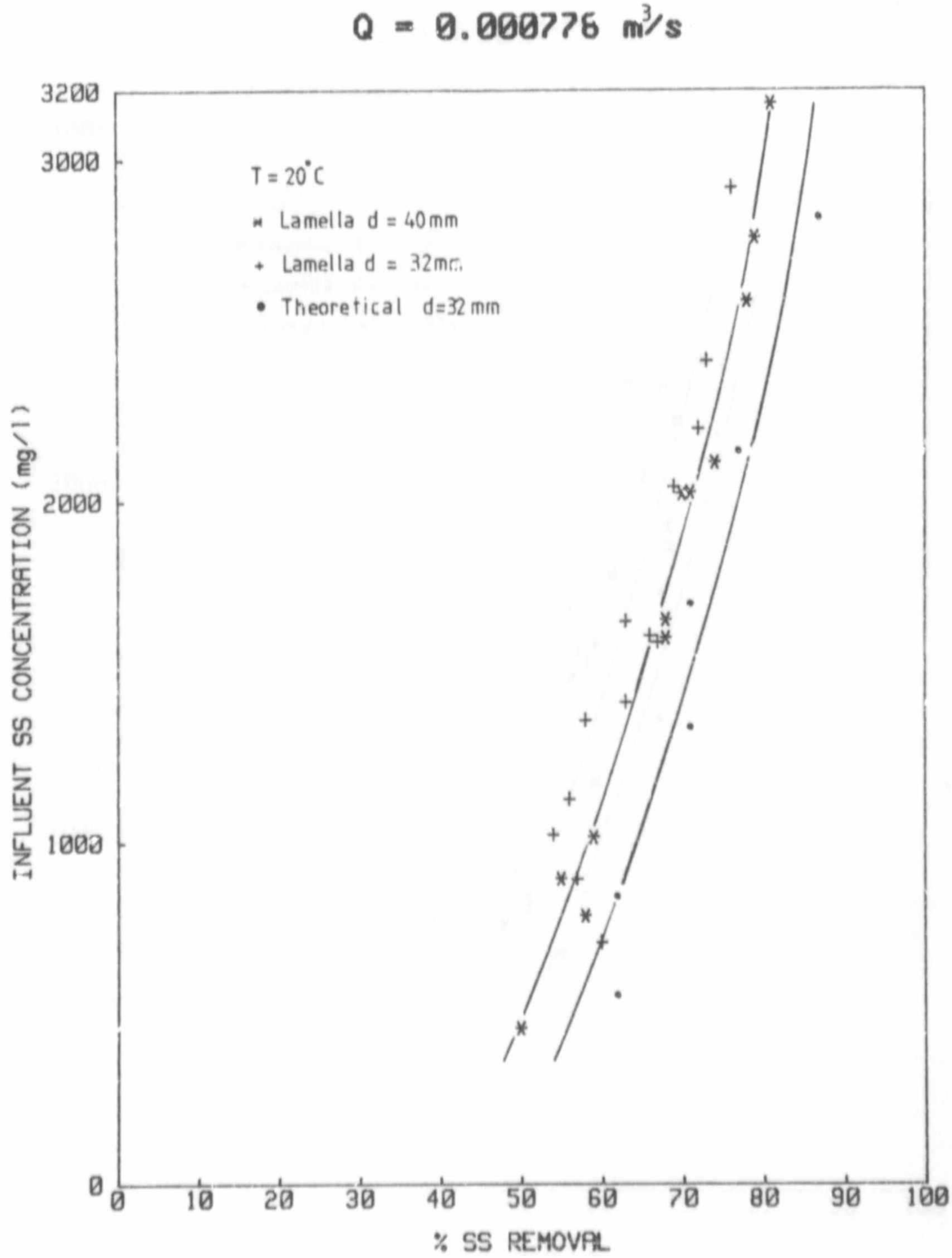

Figure 105. Influent SS concentration vs % SS removal. Q = 0,000778m³/s.

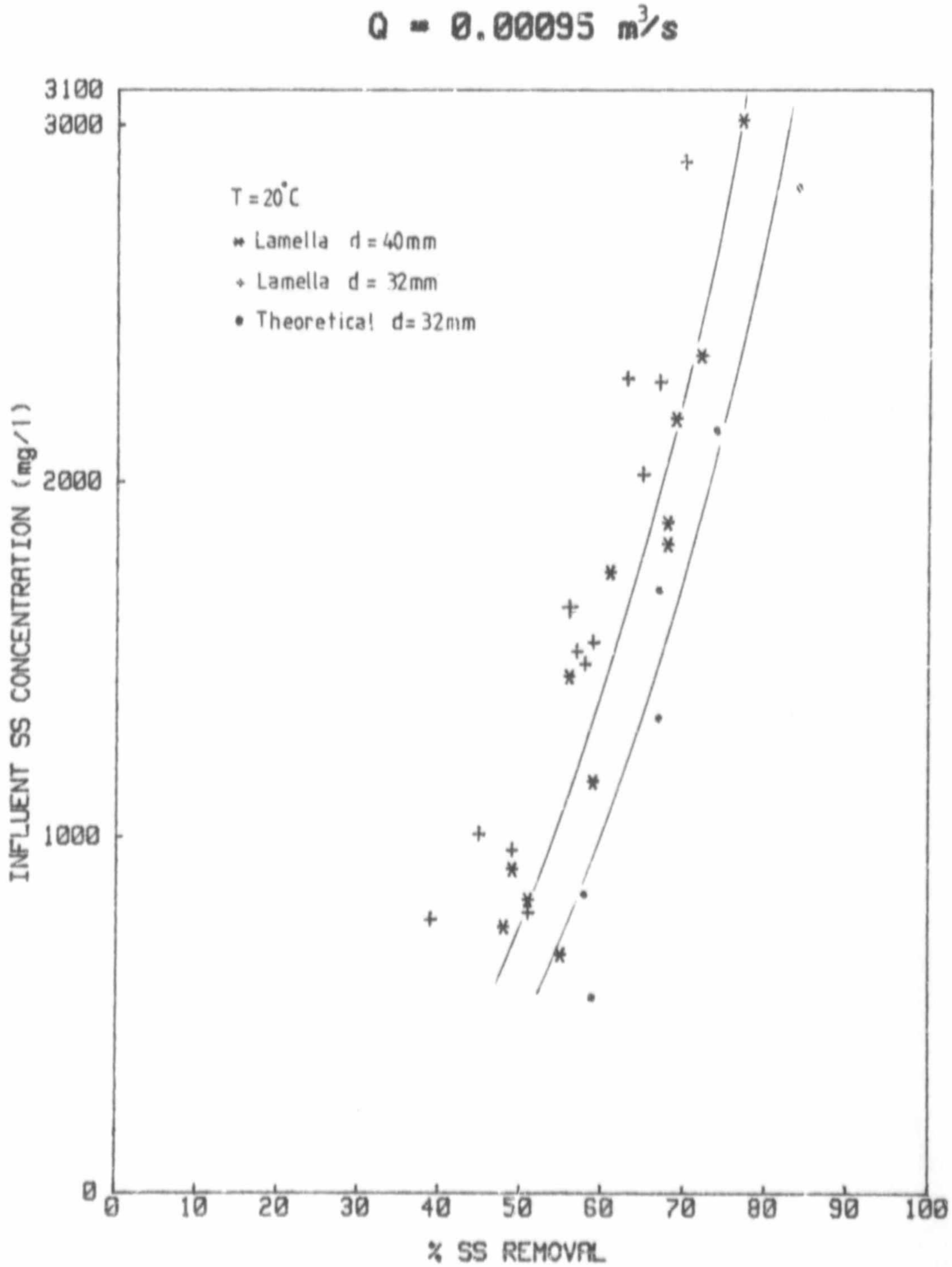

Figure 106. Influent SS concentration vs % SS removal. Q = 0,00095m³/s.

18.0 APPENDIX G. PERFORMANCE CURVES OF THE UPWARD FLOW TANK AND THE CONICAL LAMELLA SETTLER.

Curves of influent SS concentration vs % SS removed are plotted for the various upward flow tank overflow rates. Only the curves are presented for comparison (d = 40mm). The data points from which the curves where derived are given in APPENDICES C and F.

Also given are graphs of influent SS concentration vs % sludge concentration for the various upward flow tank overflow rates.

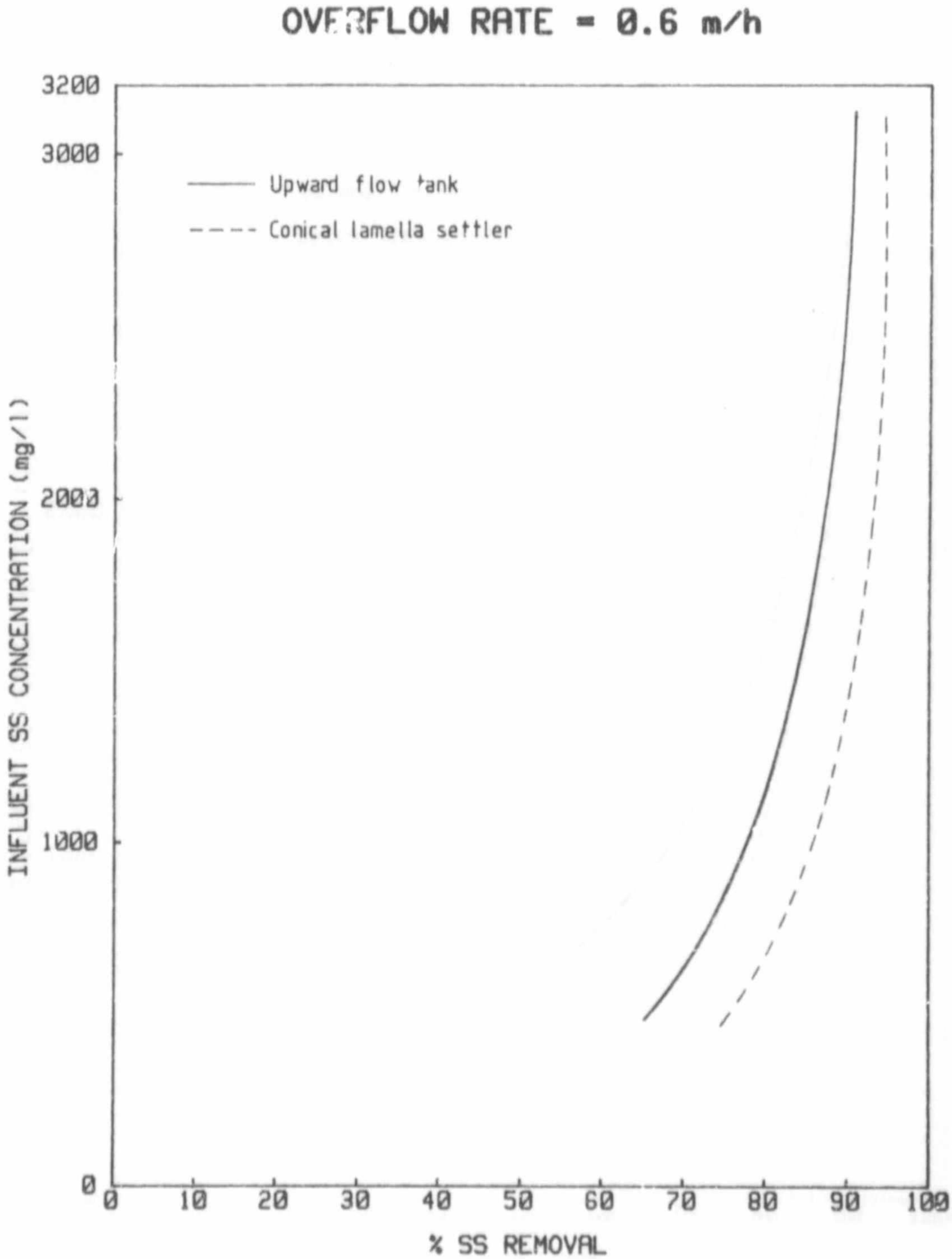

Figure 107. Upward flow and conical lamella settler performance: v = 0,6m/h.

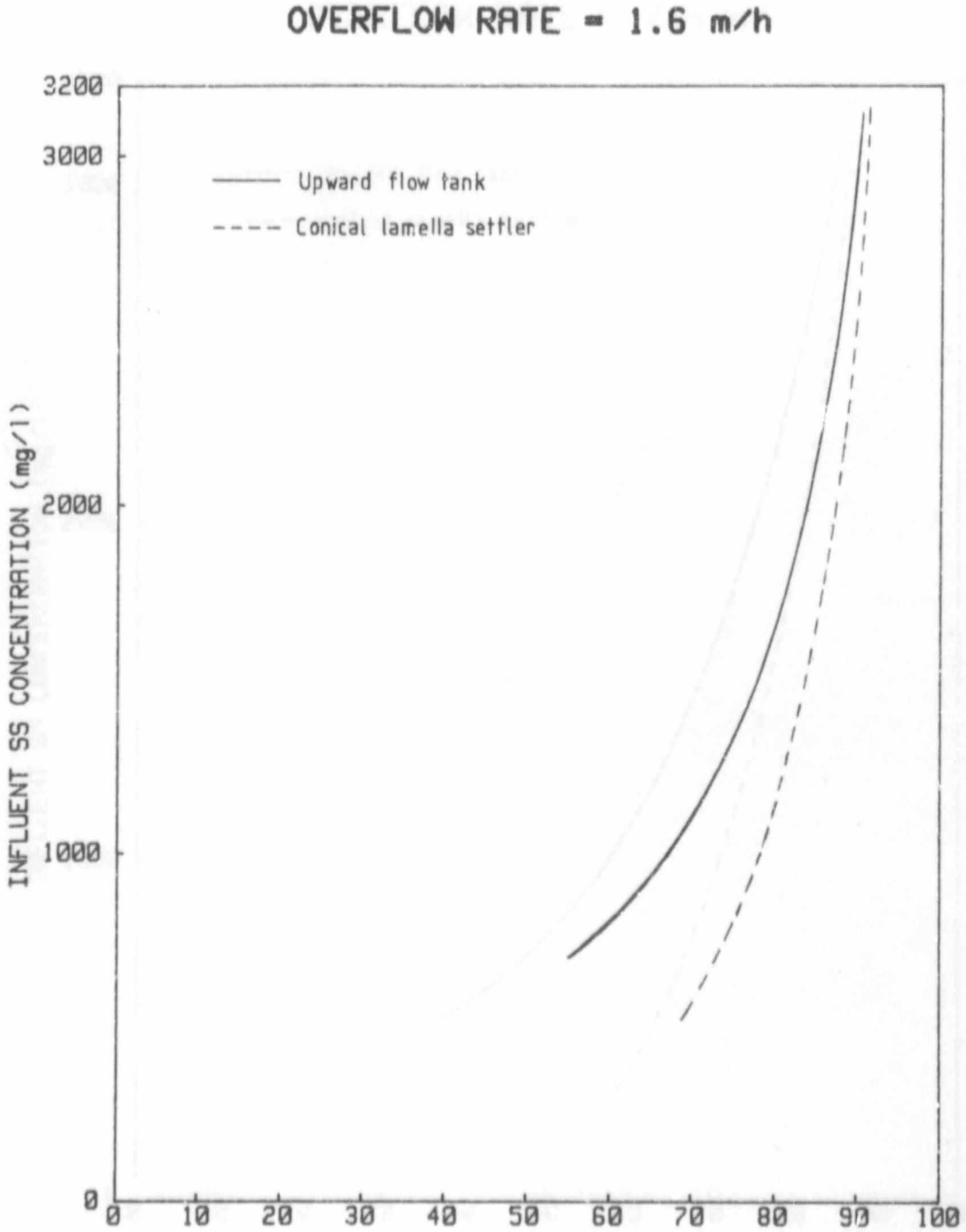

Figure 108. **Upward flow and conical lamella settler performance: v = 1,6m/h.**

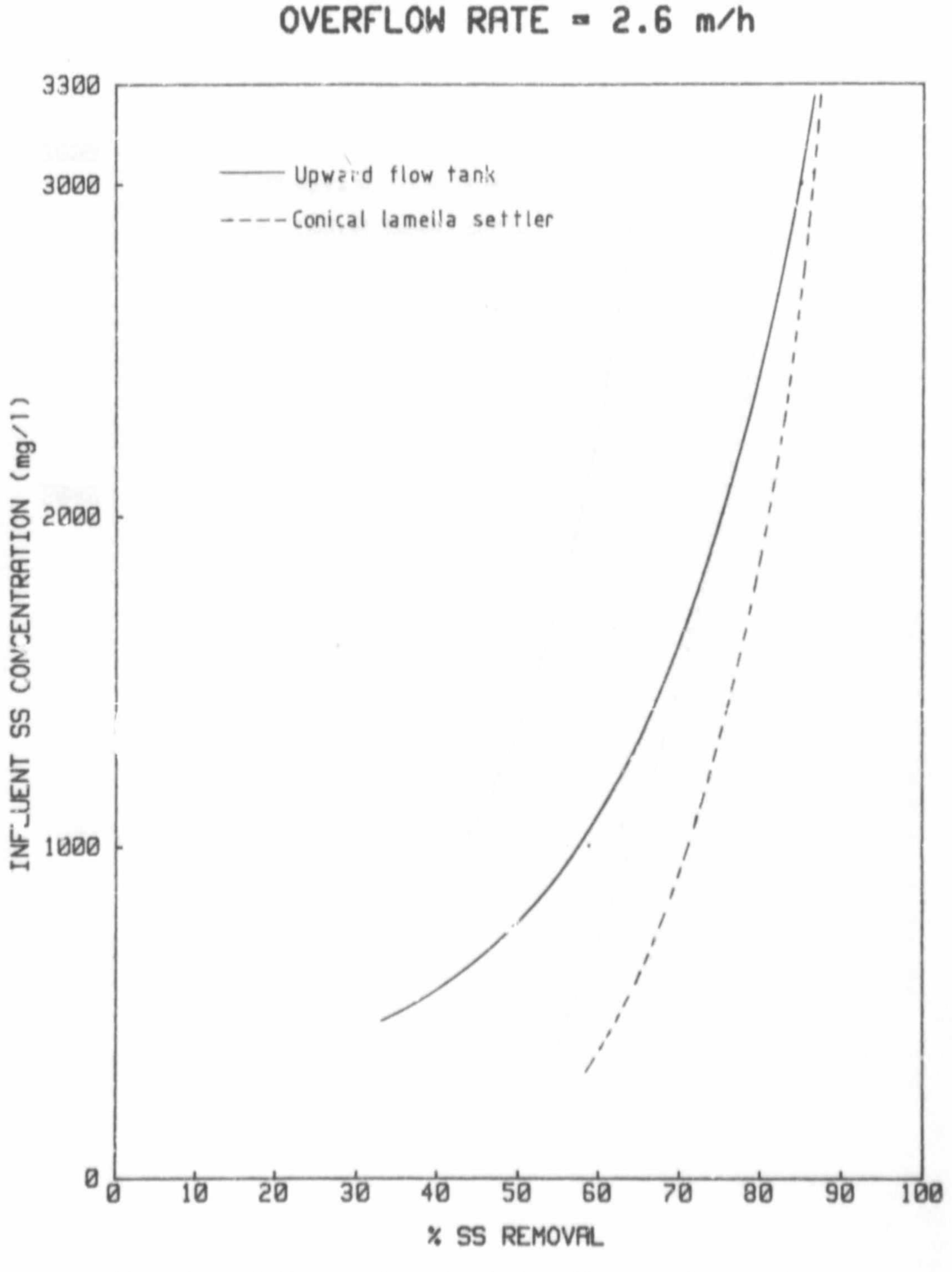

Figure 109. Upward flow and conical lamella settler performance: v = 2,6m/h.

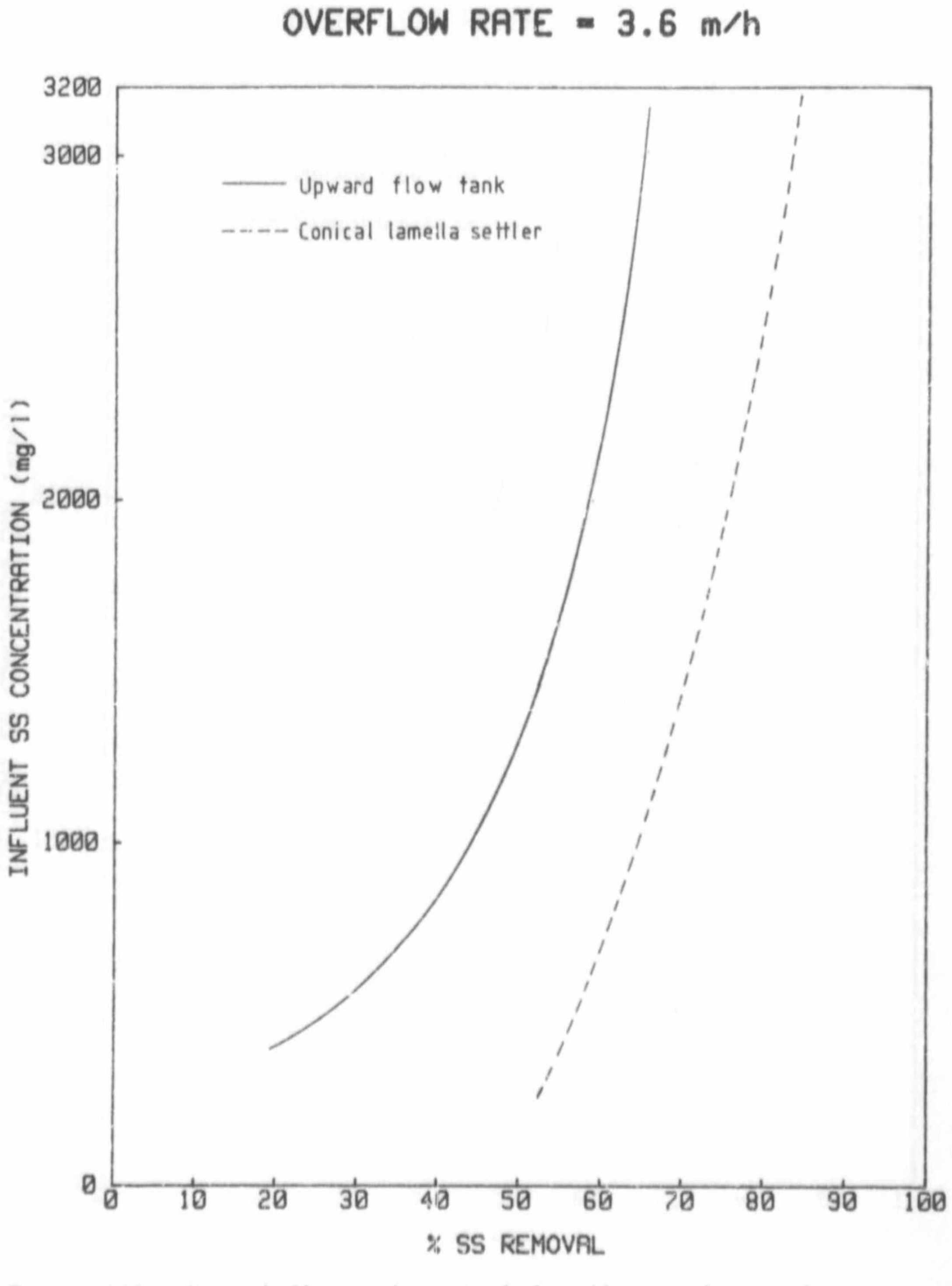

Figure 110. Upward flow and conical lamella settler performance: v = 3,6 m/h.

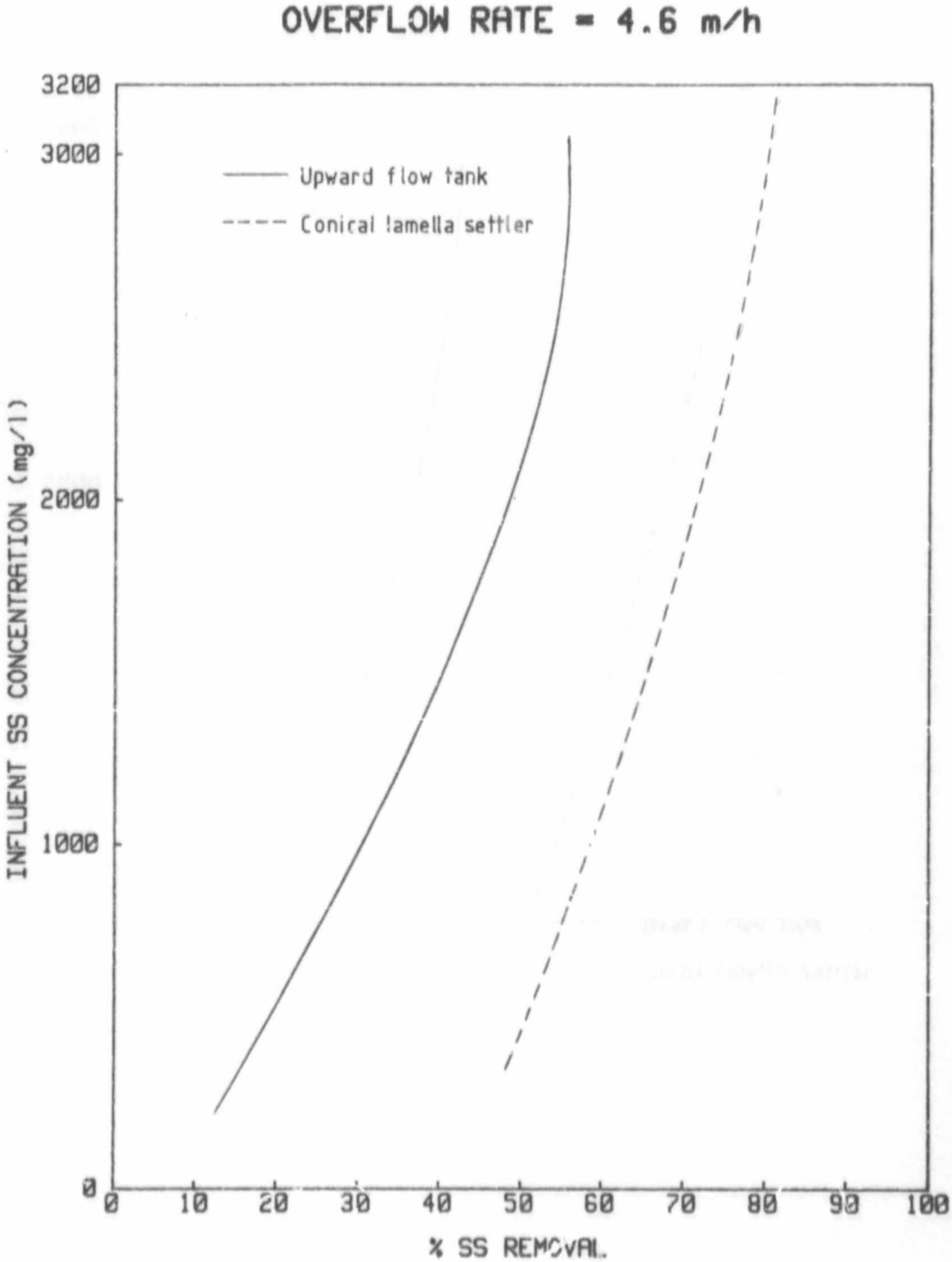

Figure 111. Upward flow and conical lamella settler performance: v = 4,6m/h.

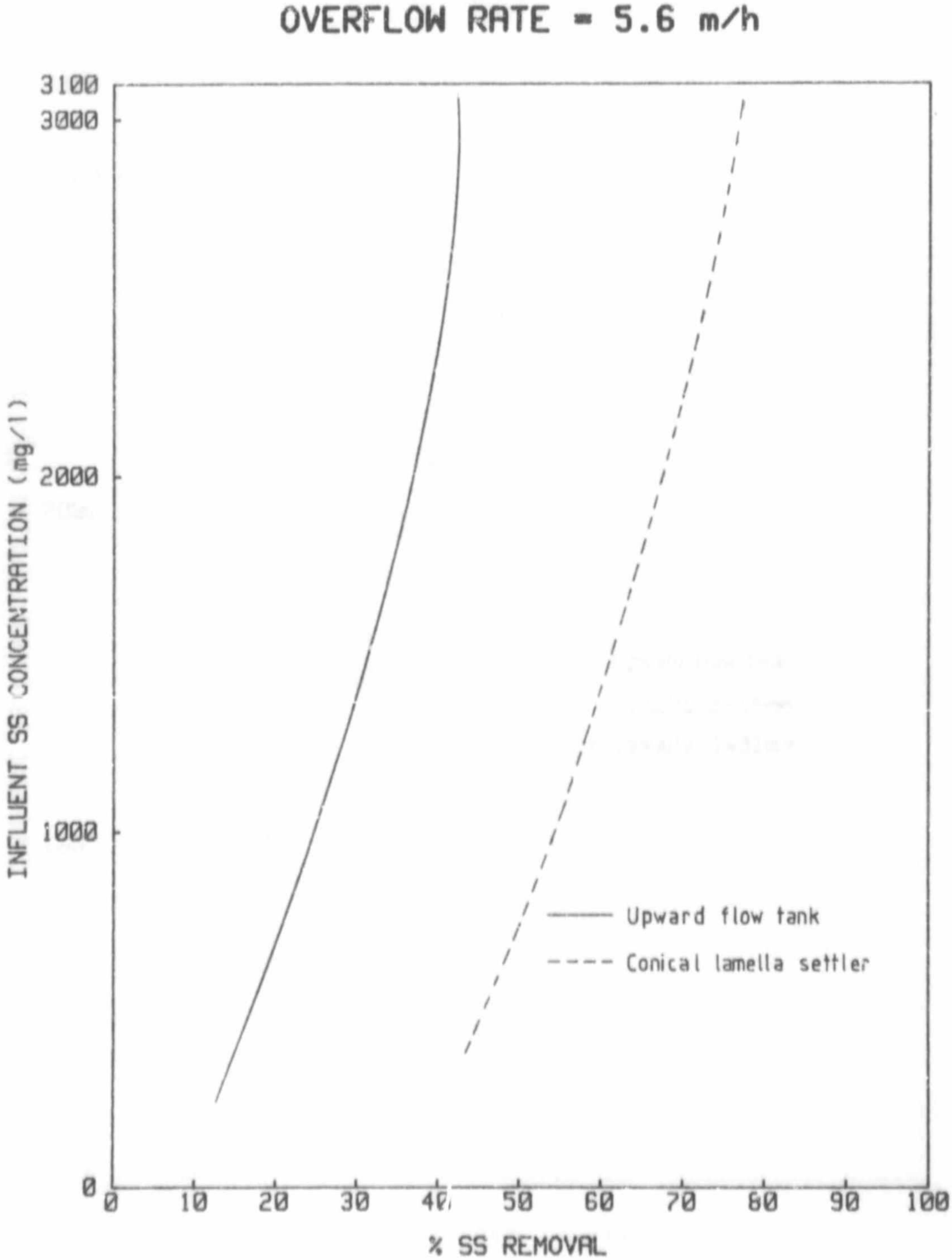

Figure 112. **Upward flow and conical lamella settler performance: v = 5,6m/h.**

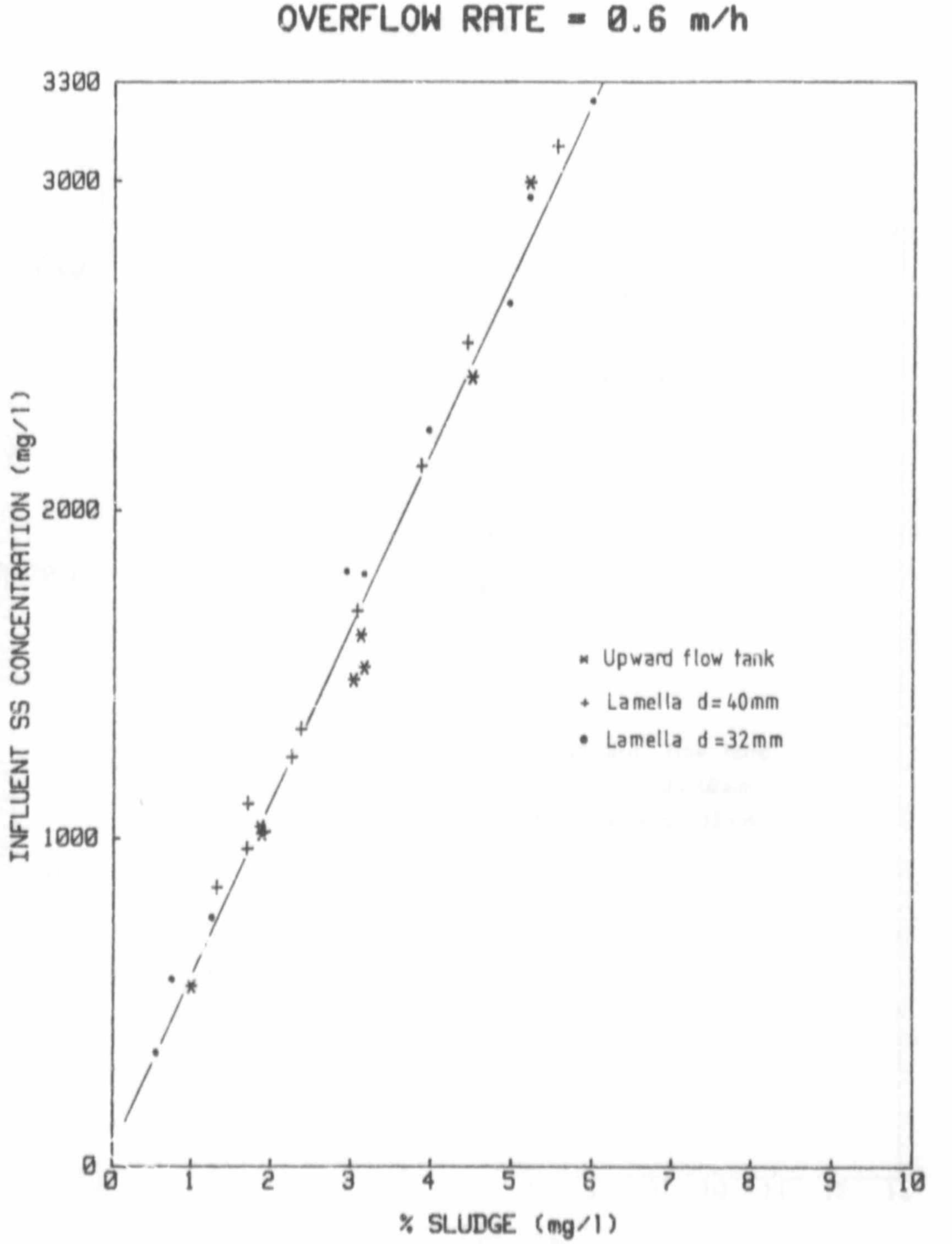

Figure 113. Influent SS concentration vs % sludge concentration: v = 0,om/h.

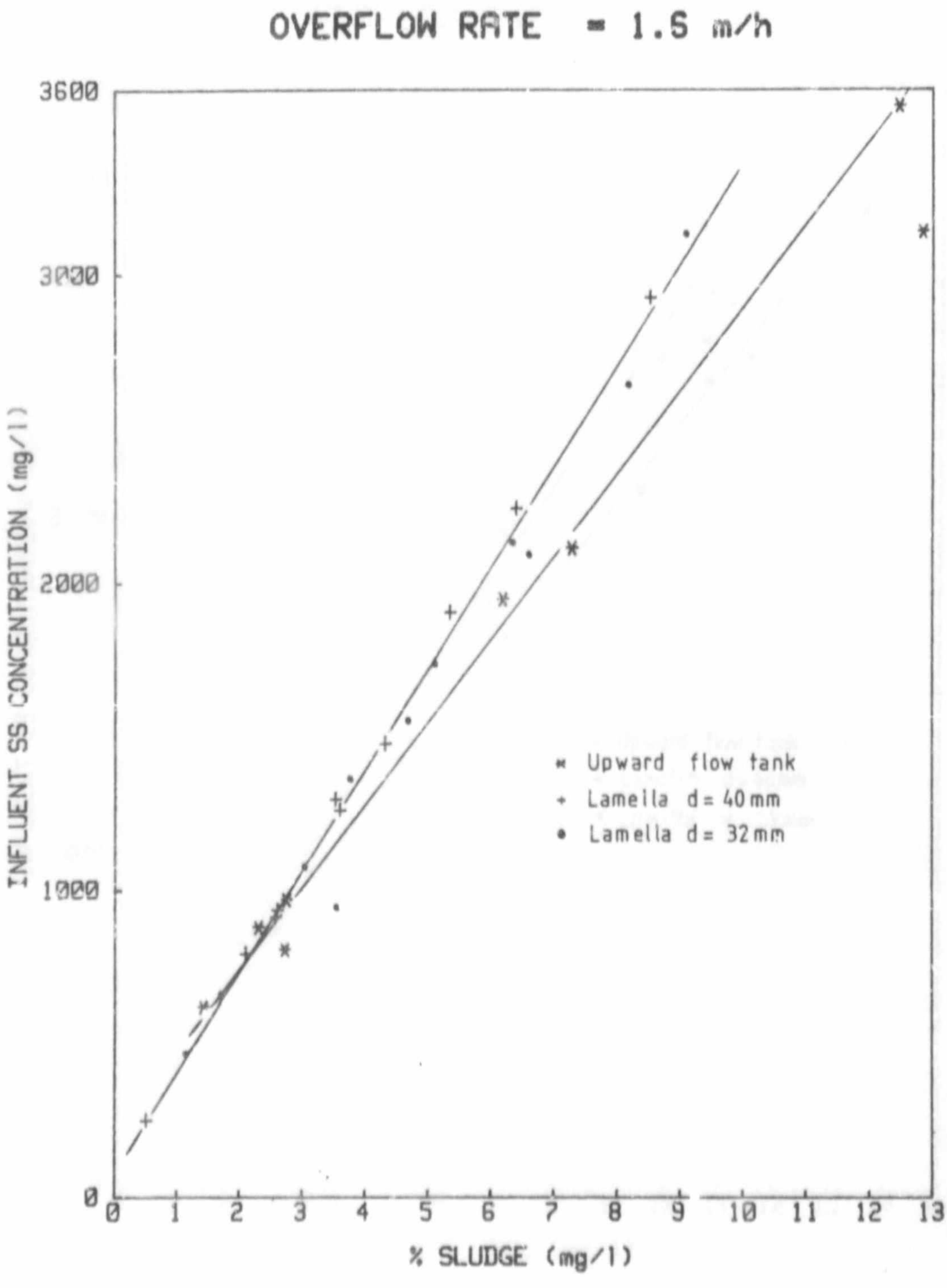

Figure 114. Influent SS concentration vs % sludge concentration: v = 1,6m/h.

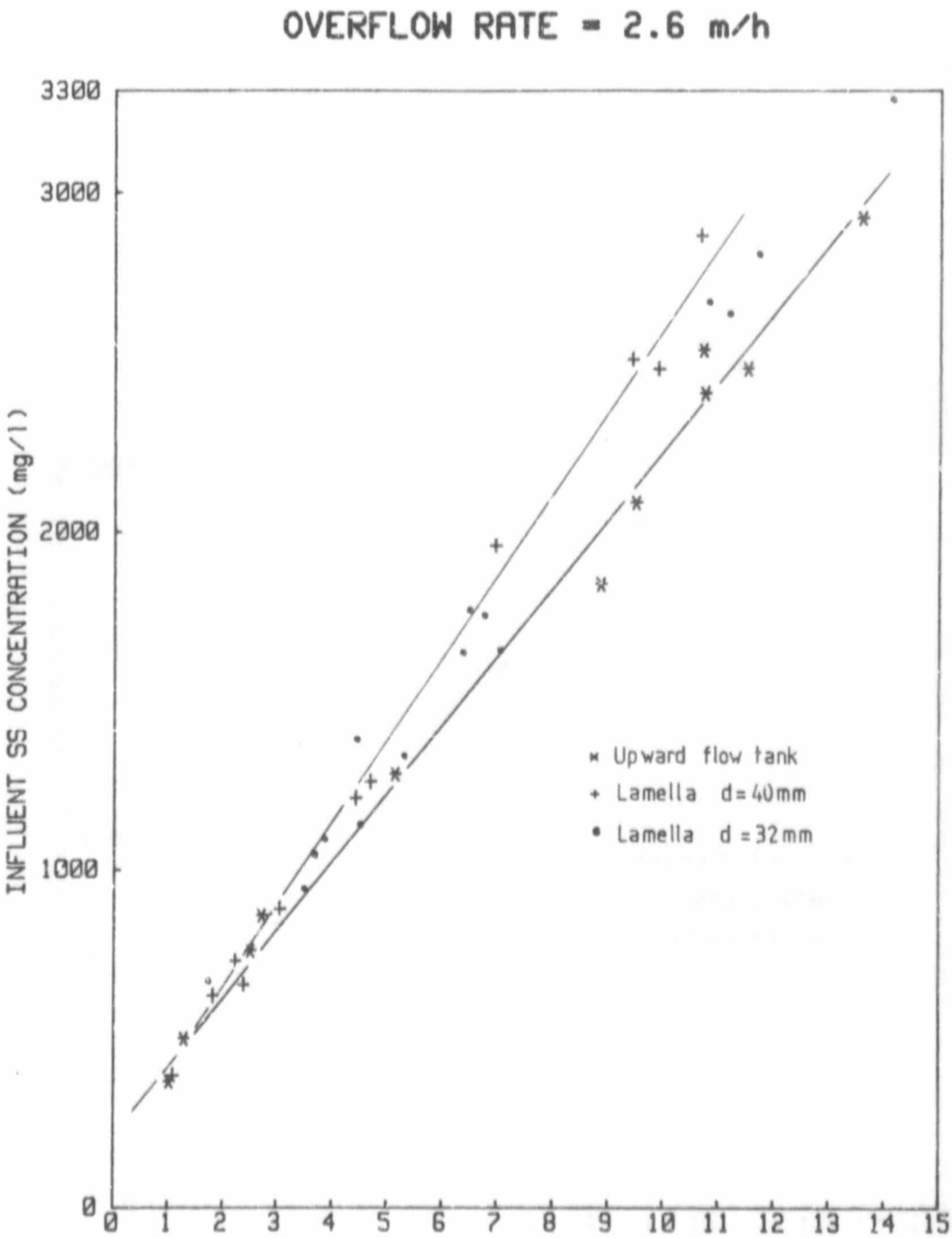

Figure 115. Influent SS concentration vs % sludge concentration: v = 2,6m/h.

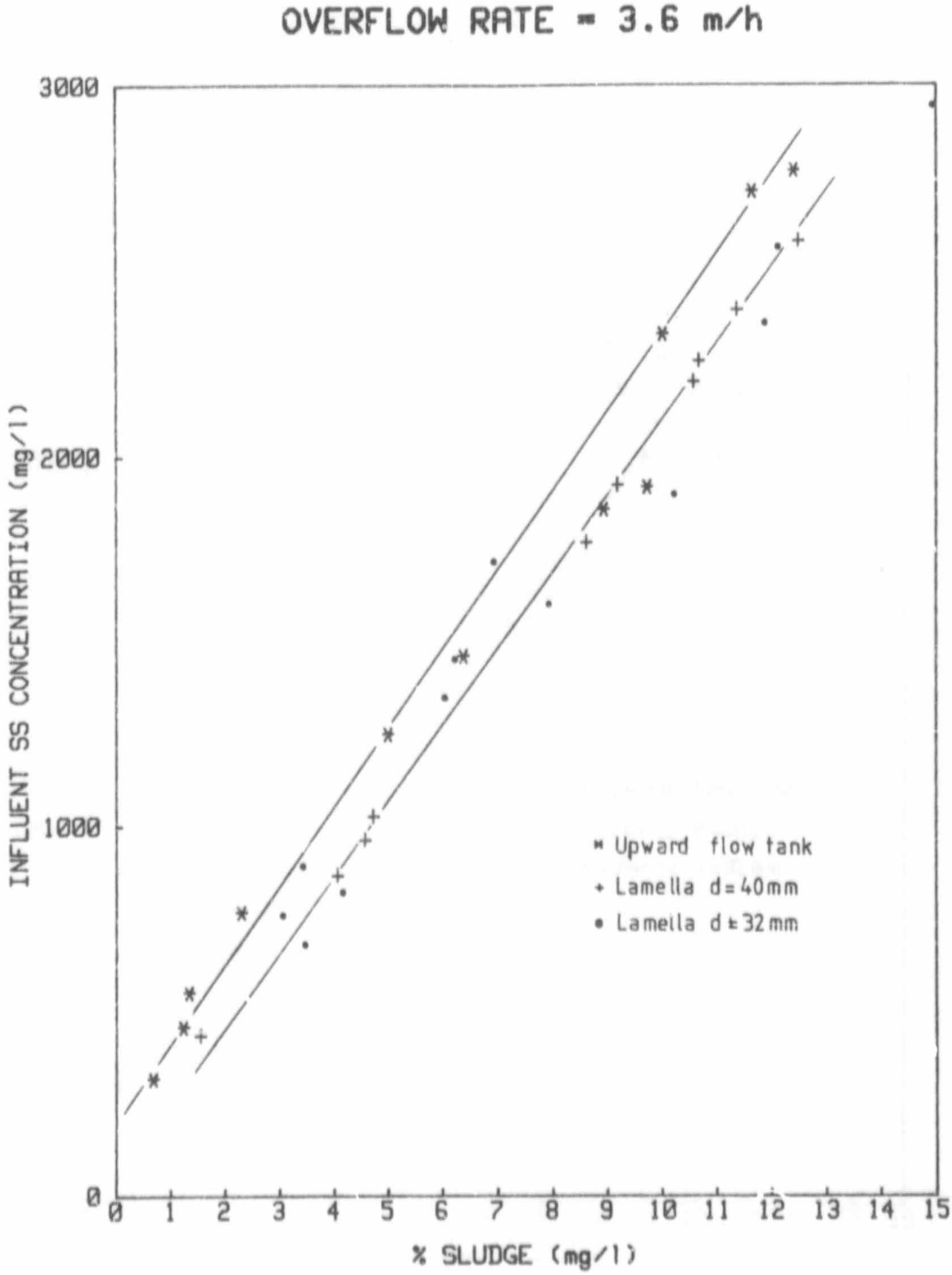

Figure 116. Influent SS concentration vs % sludge concentration: v = 3,6m/h.

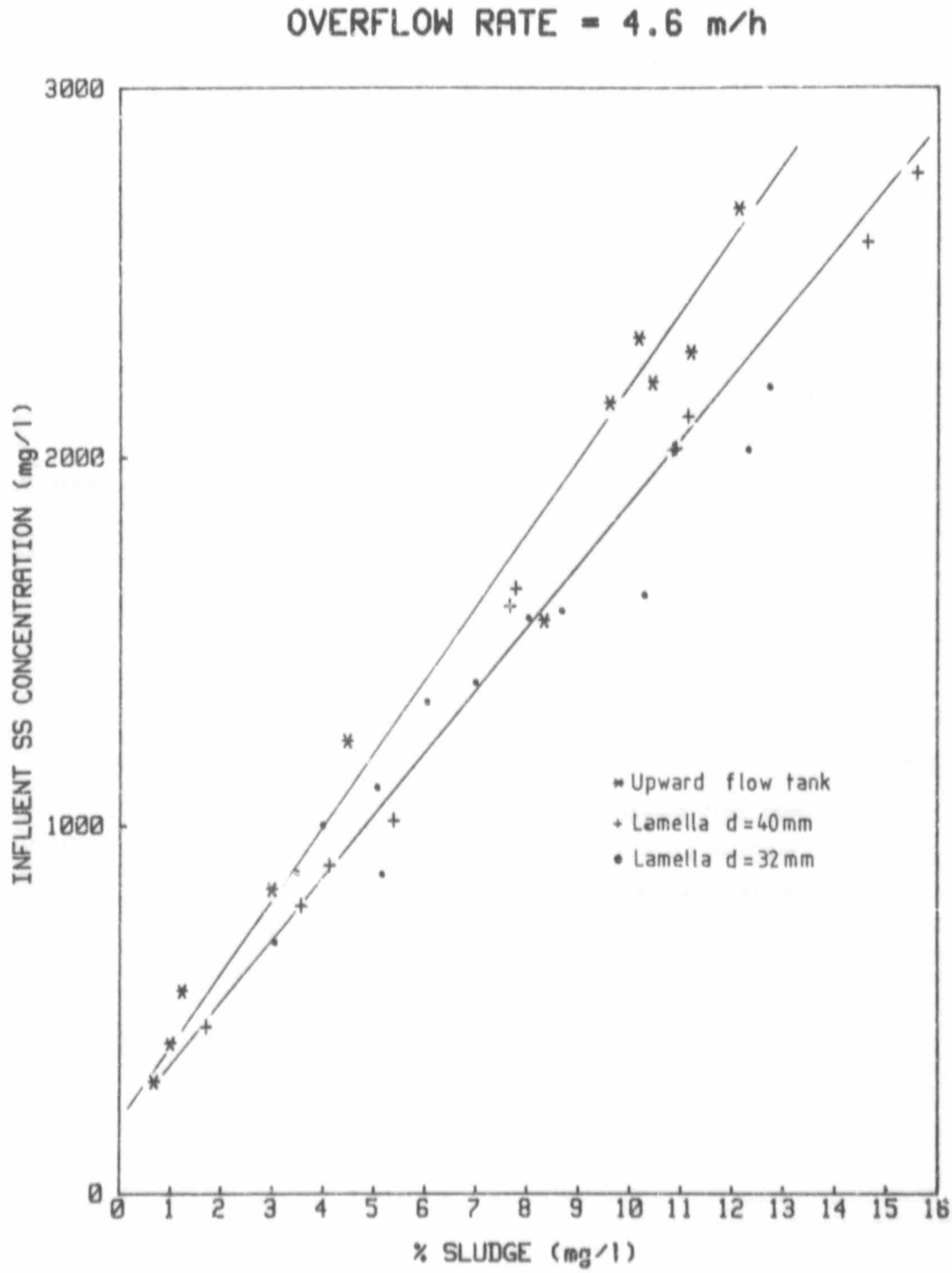

Figure 117. Influent SS concentration vs % sludge concentration: v = 4,6m/h.

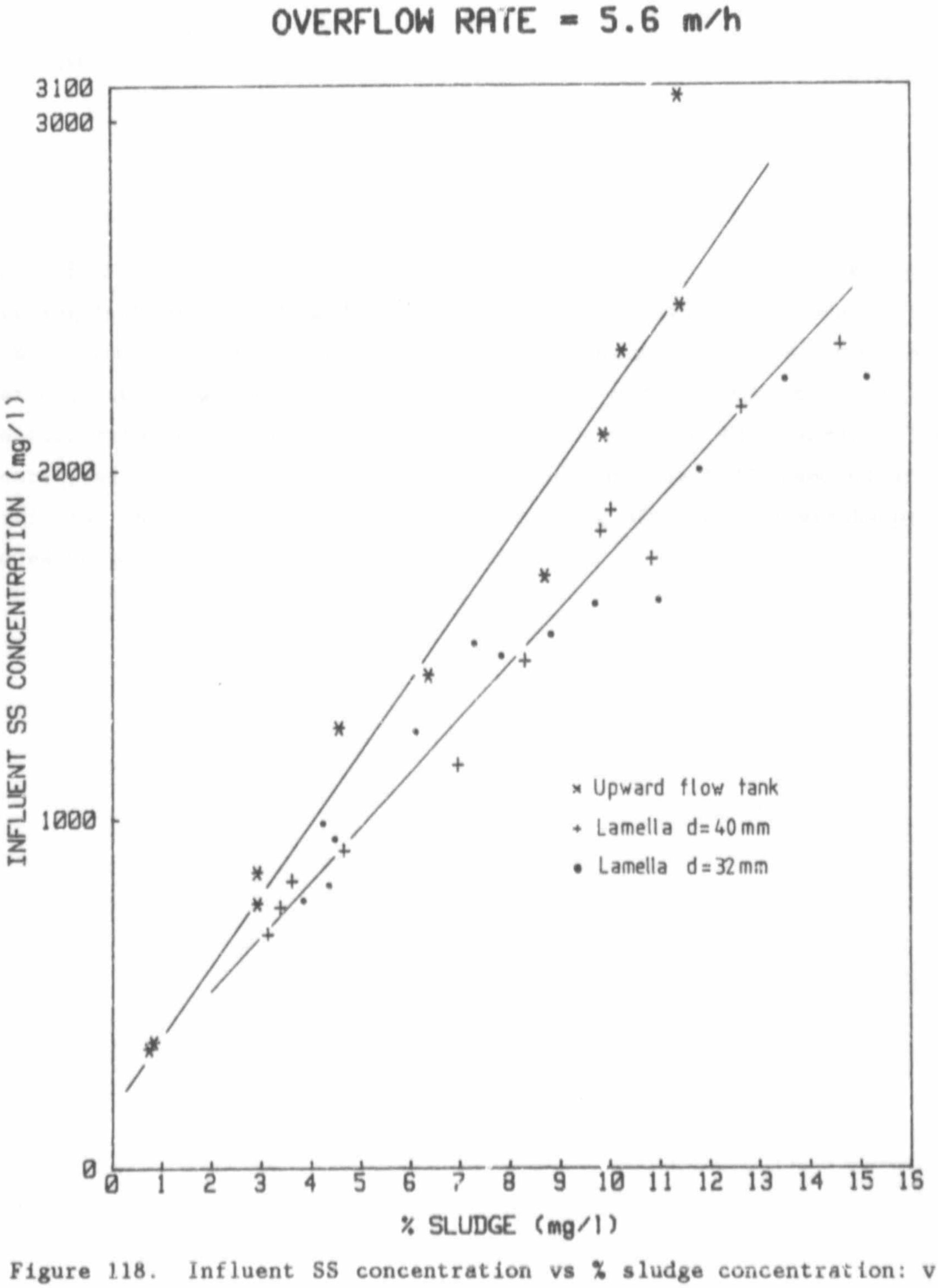

Figure 118. Influent SS concentration vs % sludge concentration: v = 5,6m/h.

19.0 APPENDIX H. BATCH SETTLING CURVES FOR H' = 0,07M AND H' = 0,056M AND THE THEORETICAL OVERFLOW RATES FOR THE VARIOUS Q.

This APPENDIX gives the curves of % SS removed vs overflow rate for a settling depth of h' = 70 and 56mm. The curves are derived from the graphs of % SS removed vs depth and time in APPENDIX A. Also given are the theoretical overflow rates (v) for the various models. Only the Model 5 overflow rates are given for a settling depth of 56mm (d = 32mm). The theoretical overflow rates are used to predict the % SS removed at a particular influent SS concentration by reading off from the graphs presented here.

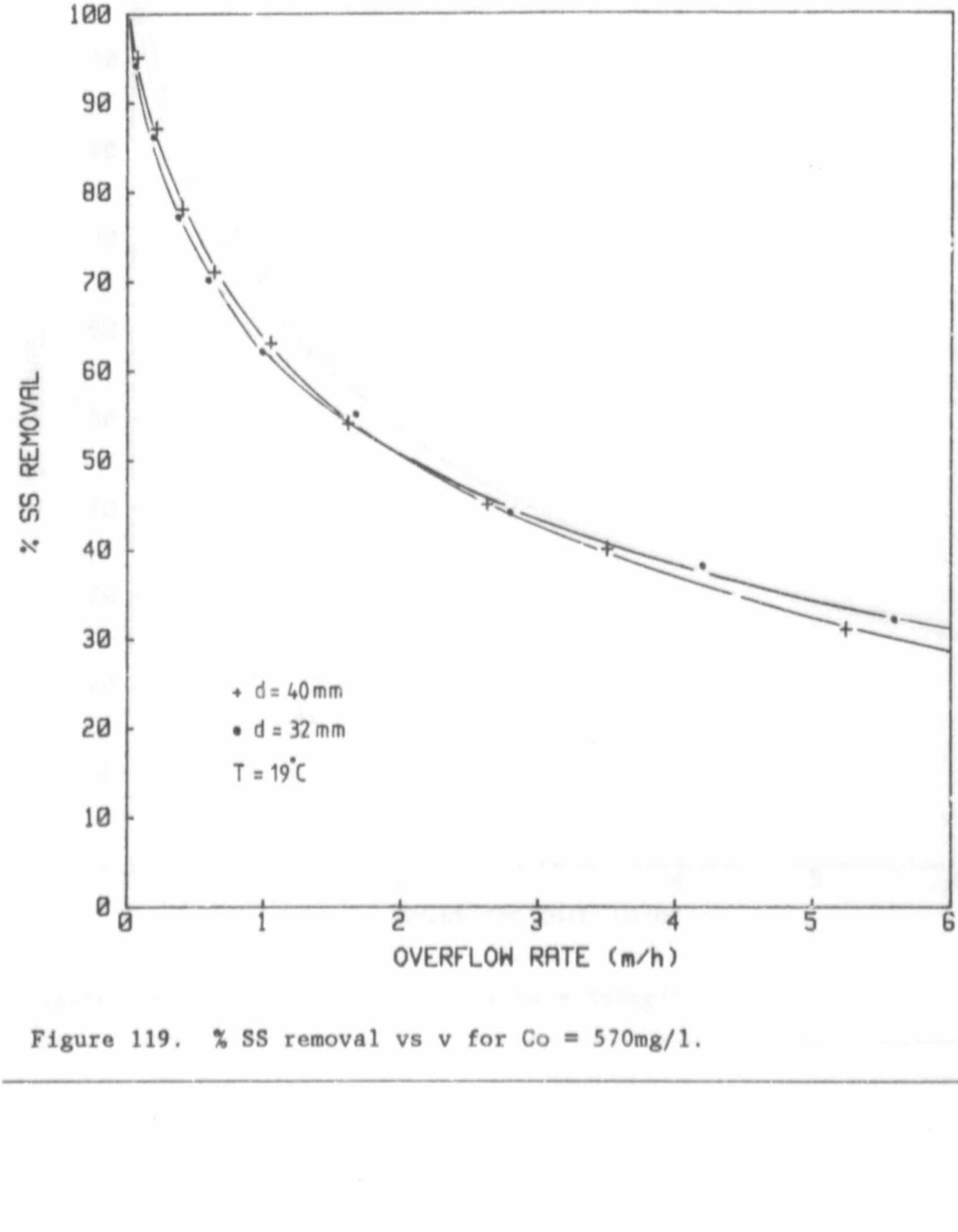

Figure 119. % SS removal vs v for Co = 570mg/l.

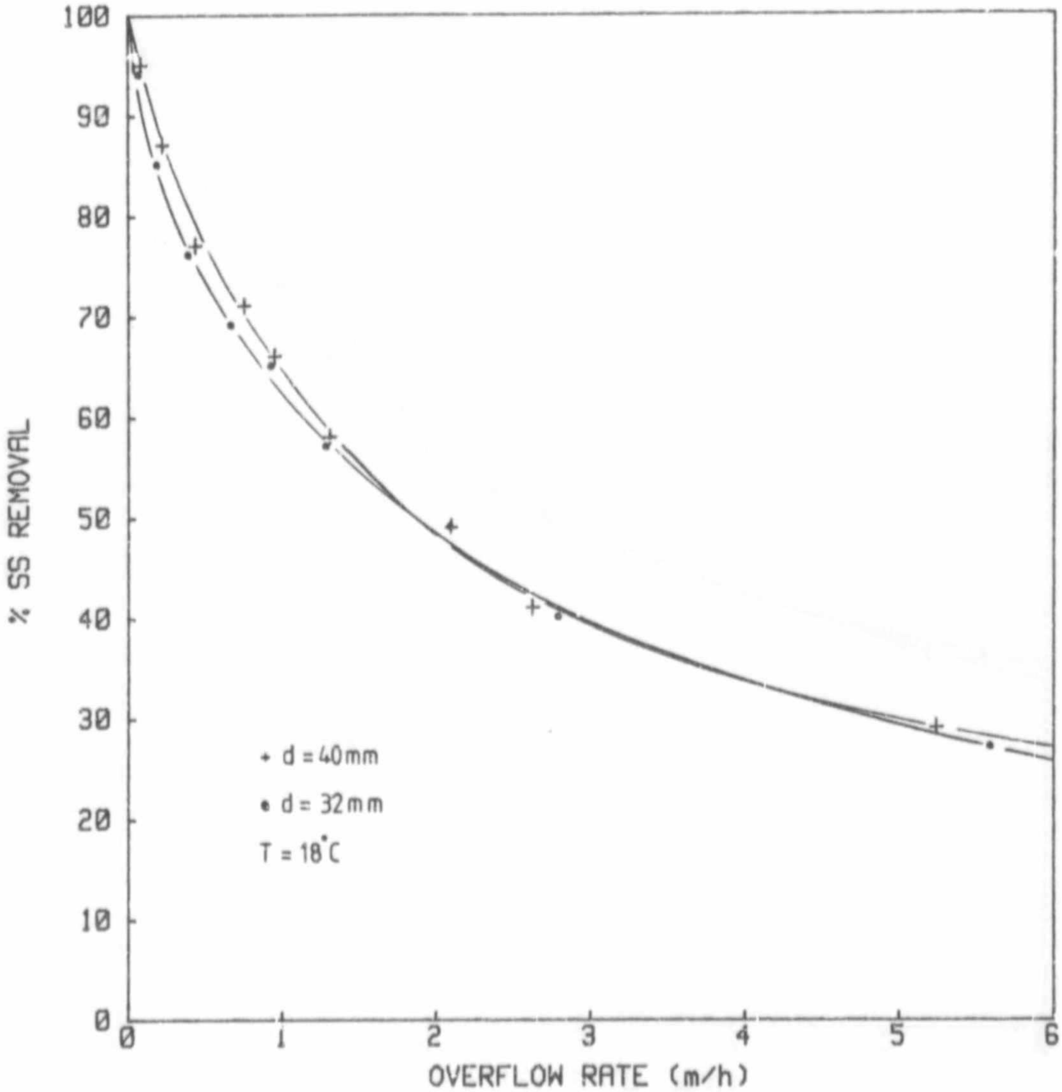

Figure 120. % SS removal vs v for Co = 860mg/1.

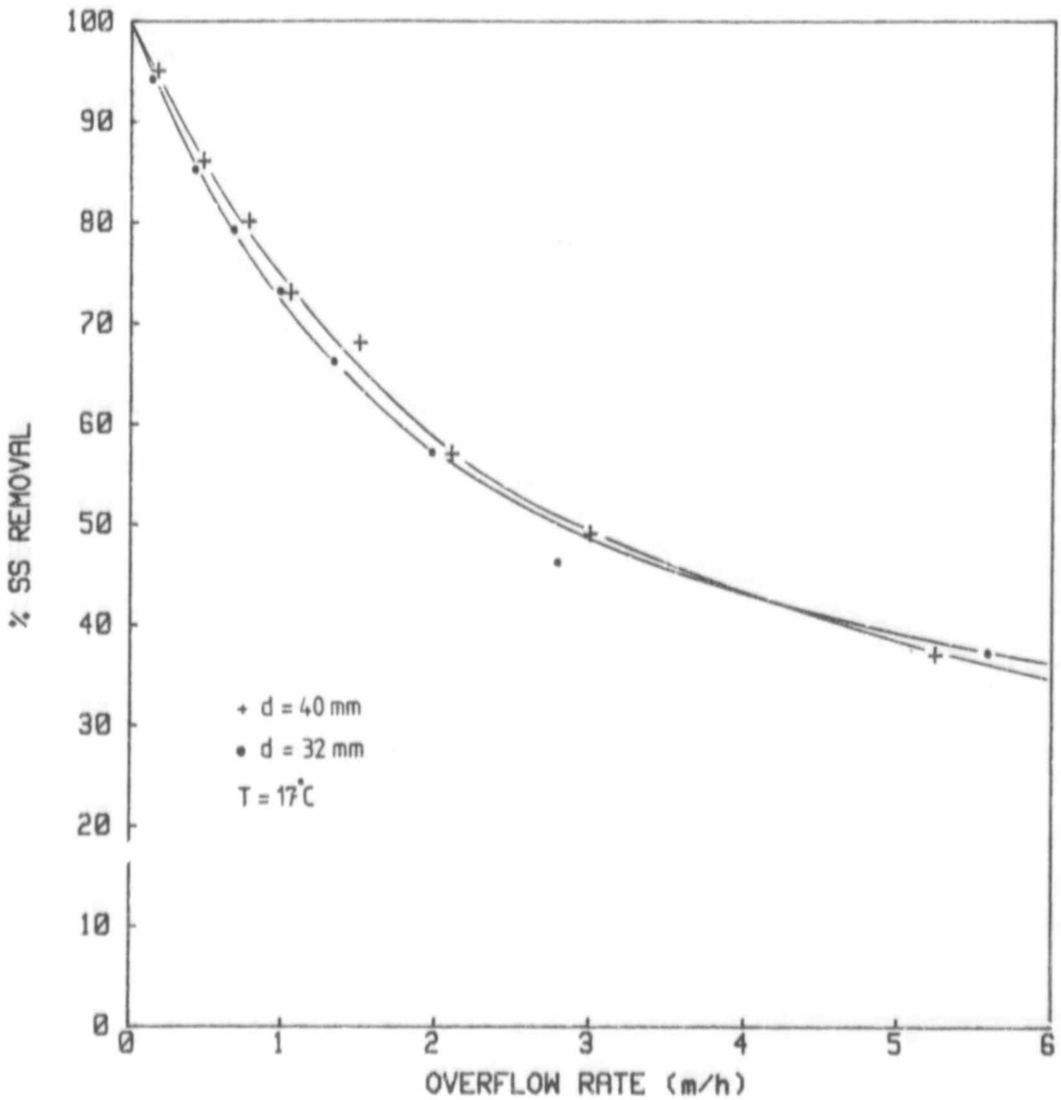

Figure 121. % SS removal vs v for Co = 1356mg/l.

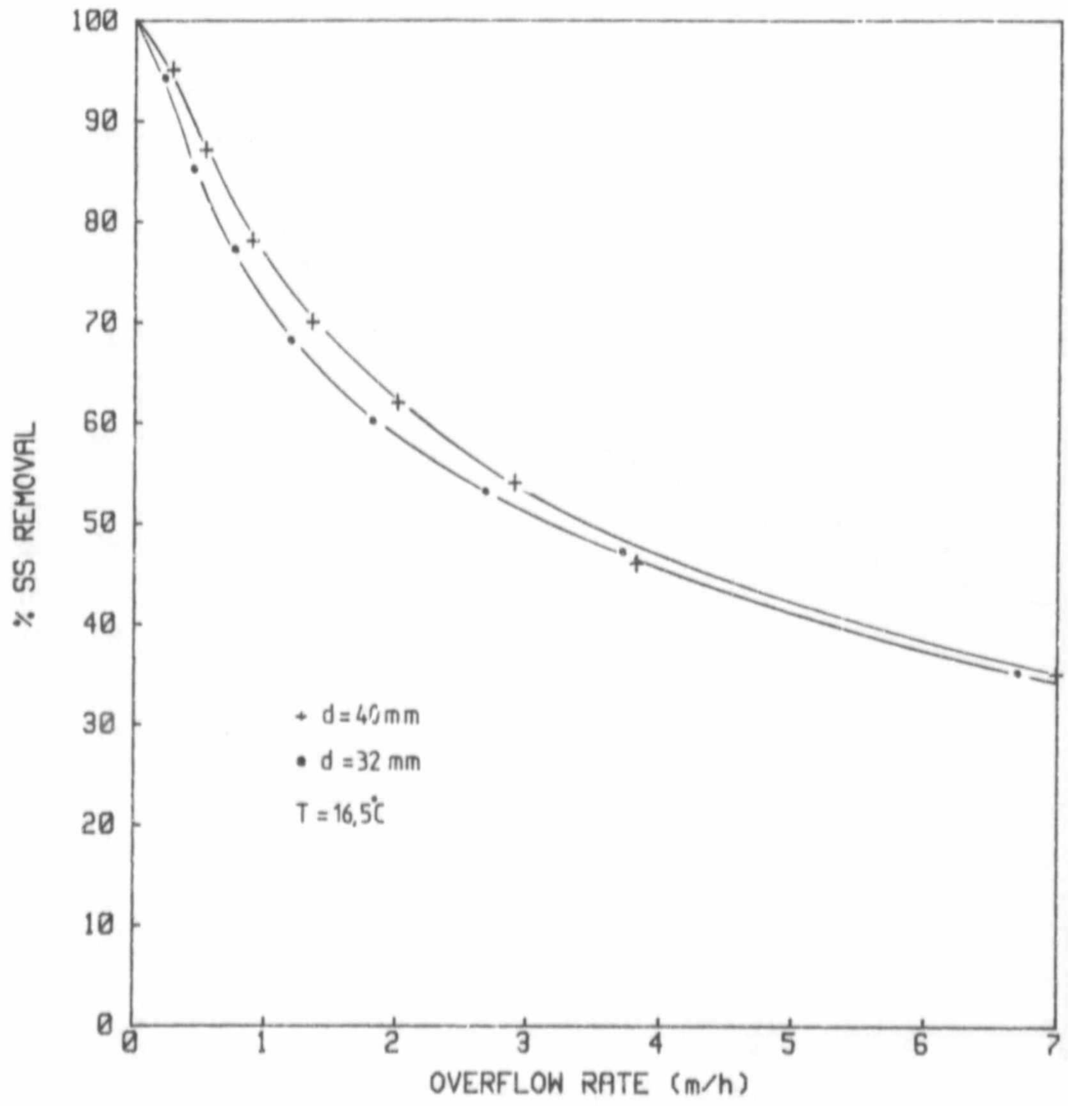

Figure 122. % SS removal vs v for Co = 1717mg/l.

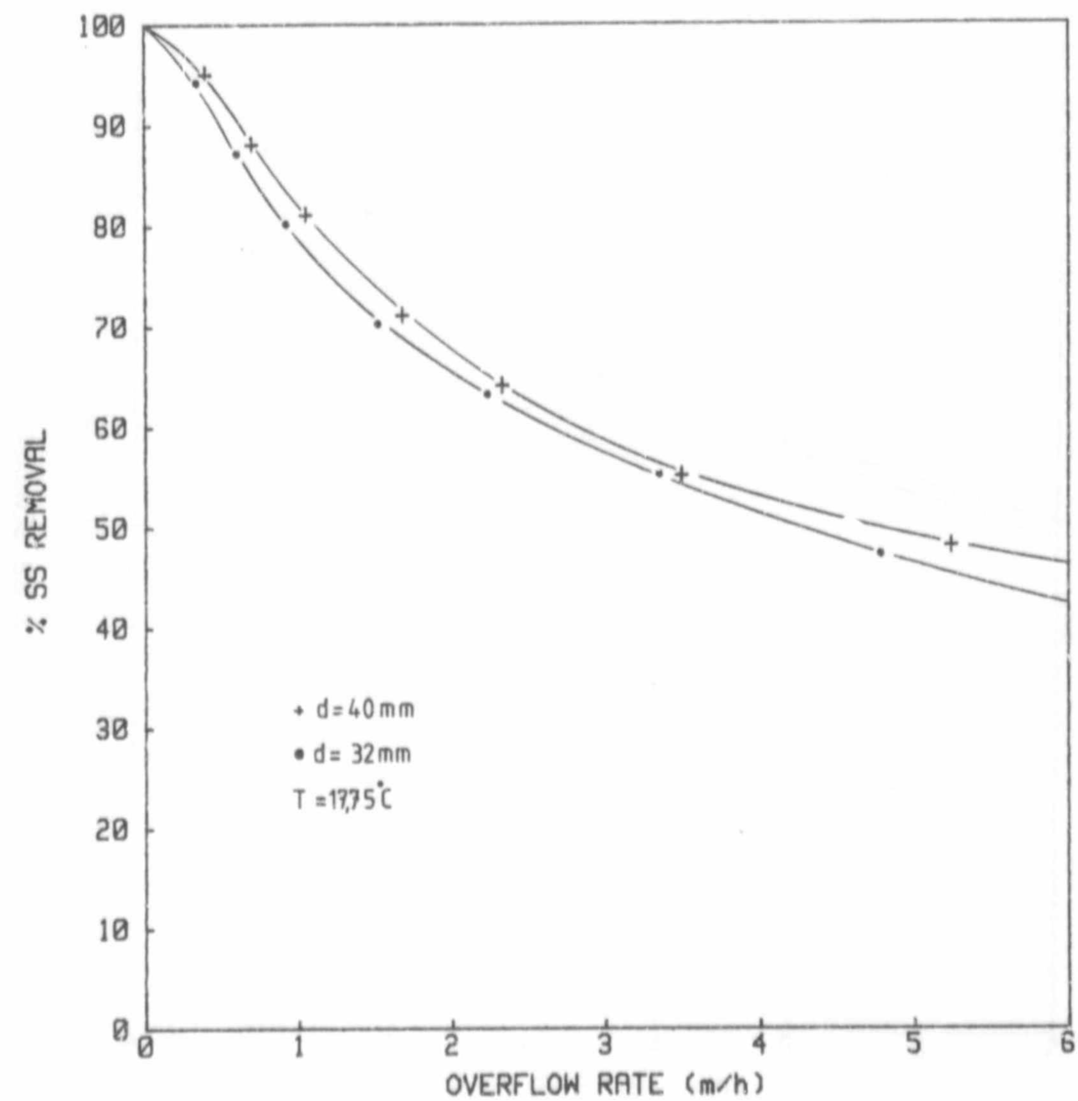

Figure 123. % SS removal vs v for Co = 2164mg/l.

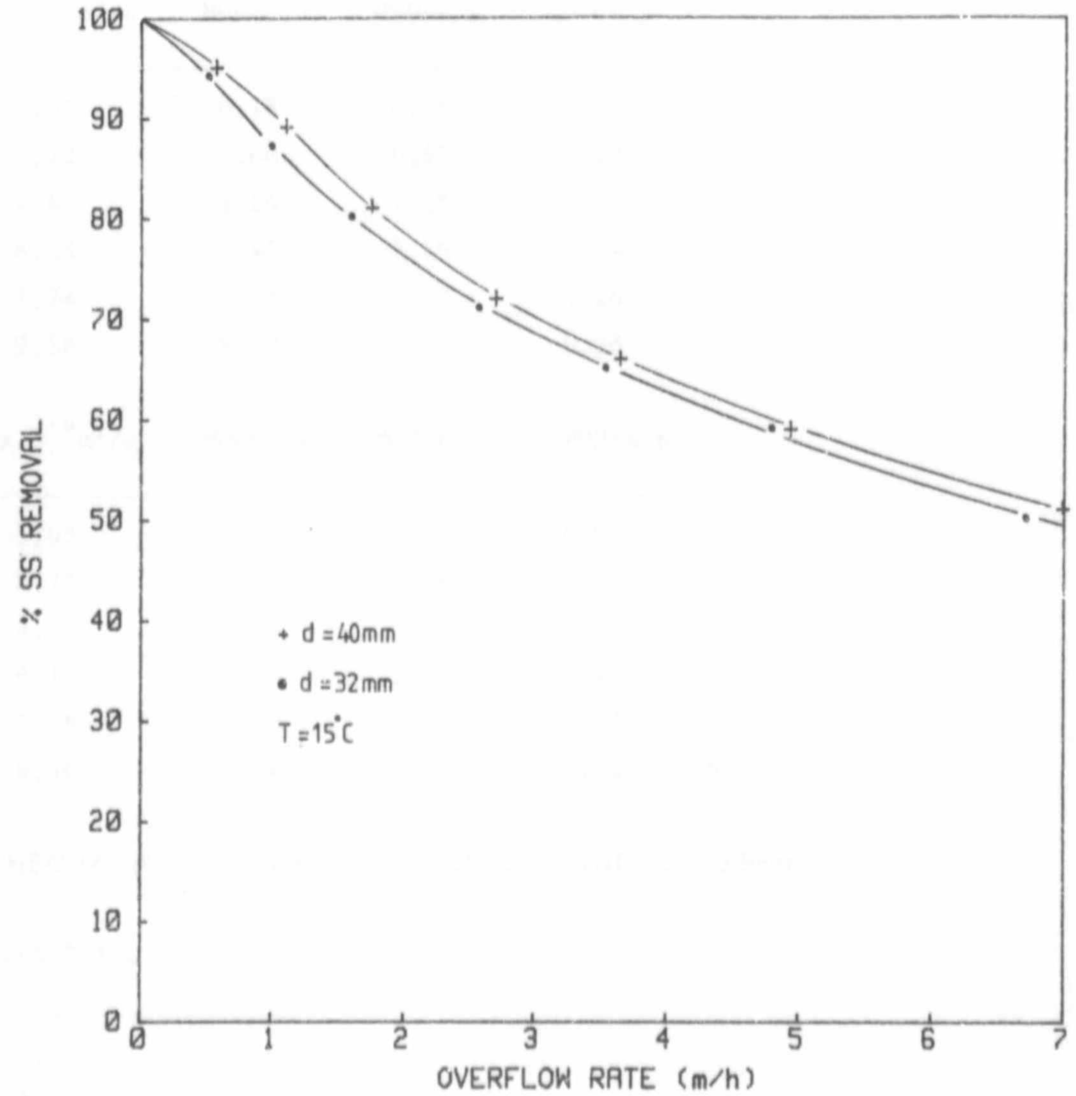

Figure 124. % SS removal vs v for Co = 2846mg/l.

THEORETICAL v(m/h) FOR THE VARIOUS MODELS AND d = 40mm

$Qx10^{-4}m^3/s$	MODEL 1	MODEL 2	MODEL 3
1,03	0,18	0,18	0,041
2,72	0,60	0,60	0,13
4,42	1,26	1,15	0,27
6,11	2,48	1,59	0,54
7,78	5,48	2,02	1,20
9,50	28,77	2,47	6,28

$Qx10^{-4}m^3/s$	MODEL 4	MODEL 5	MODEL 6
1,03	0,041	0,17	0,04
2,72	0,13	0,46	0,10
4,42	0,25	0,75	0,16
6,11	0,35	1,03	0,23
7,78	0,44	1,31	0,29
9,50	0,54	1,60	0,35

THEORETICAL v(m/h) FOR MODEL 5 AND d = 32mm.

$Qx10^{-4}m^3/s$	MODEL 5
1,03	0,14
2,72	0,38
4,42	0,61
6.11	0,85
7,78	1,08
9,50	1,32

APPENDIX H. BATCH SETTLING CURVES FOR h' = 0,07m AND h' = 0,056m AND THE THEORETICAL OVERFLOW RATES FOR THE VARIOUS Q.

20.0 APPENDIX I. DERIVATION OF THE VOLUME BETWEEN TWO CONICAL SURFACES AND THE NAKAMURA MODEL FOR CONES.

Two derivations are given in this APPENDIX. The first concerns the Yao(1970) model and consists of deriving the volume between two conical plates. The second converts the Nakamura model for quiescent settling conditions under inclined rectangular plates into a model which can be used for conical plates.

Volume between two conical plates.

The volume of a frustum of a cone is given as:

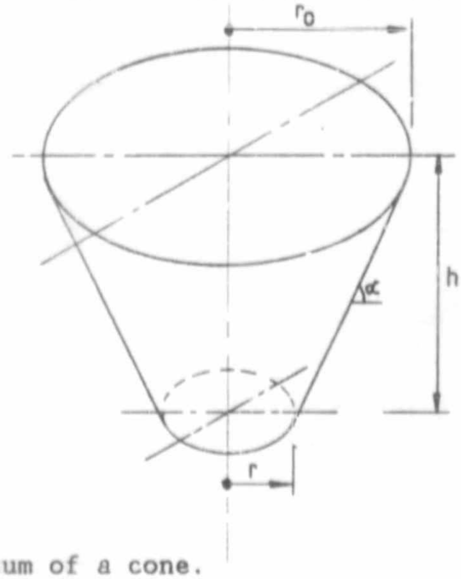

Figure 125. Frustum of a cone.

$$V = \pi h/3.[\ (r_0)^2 + r_0.r + r^2\ ]$$

and $h = (r_0 - r)\tan\alpha$

hence $V = \pi\tan\alpha/3[\ r_0 - r\ ].[\ (r_0)^2 + r_0.r + r^2\ ]$

TRANSITION LENGTH VOLUME:

Volume between two frustums of cones taking r_0 as the radius to the end of the transition length:

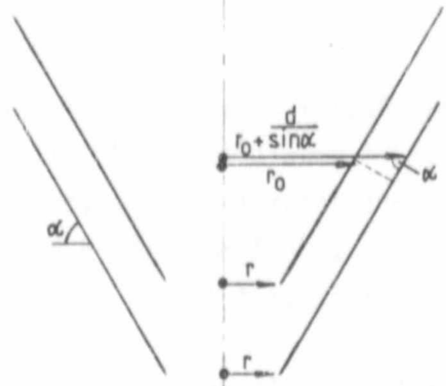

Figure 126. Dimensions of the transition length.

The volume obtained by subtracting the inner frustum cone from the outer frustum is as follows:

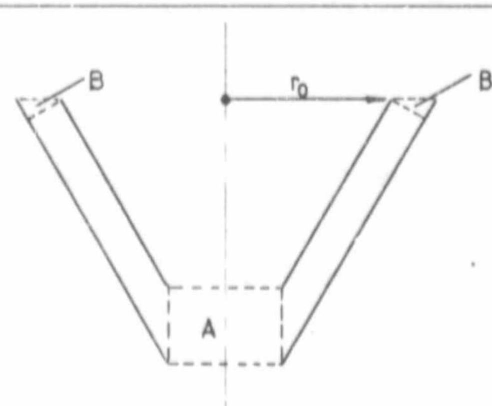

Figure 127. Schematic representation of the remaining volume between two frustums.

$$\text{Total volume} = \pi\tan\alpha/3[\{ r_0 + d/\sin\alpha - r \}.\{ (r_0+d/\sin\alpha)^2 + (r_0+d/\sin\alpha)r + r^2 \} - \{r_0-r\}.\{ (r_0)^2 + r_0.r$$

$$+ r^2 \}]$$

Expanding:

$$V_T = \pi\tan\alpha/3[\{ r_0 + d/\sin\alpha - r \}.\{ (r_0)^2 + 2r_0 d/\sin\alpha + d^2/(\sin\alpha)^2 + r_0.r + rd/\sin\alpha + r^2 \} - \{r_0 - r\}.\{ (r_0)^2 + r_0.r + r^2 \}]$$

$$= \pi\tan\alpha/3[(r_0)^3 + 2(r_0)^2 d/\sin\alpha + r_0 d^2/(\sin\alpha)^2 + (r_0)^2 r + r_0 rd/\sin\alpha + r_0.r^2 + (r_0)^2 d/\sin\alpha + 2r_0.d^2/(\sin\alpha)^2 + d^3/(\sin\alpha)^3 + r_0 r.d/\sin\alpha + rd^2/(\sin\alpha)^2 + r^2 d/\sin\alpha - r.(r_0)^2 - 2r.r_0 d/\sin\alpha - r.d^2/(\sin\alpha)^2 - r_0.r^2 - r^2 d/\sin\alpha - r^3 - (r_0)^3 - (r_0)^2.r - r_0.r^2 + r(r_0)^2 + r_0.r^2 + r^3]$$

$$V_T = \pi\tan\alpha/3[3(r_0)^2 d/\sin\alpha + 3r_0 d^2/(\sin\alpha)^2 + d^3/(\sin\alpha)^3]$$

Volumes A and B in the above figure still have to be subtracted from V_T to give the actual volume between the plates for radii r and r_0:

$$V_A = \pi r^2.d/\cos\alpha$$

$$V_B = \tfrac{1}{2}d^2.2\pi r_0/\tan\alpha = \pi d^2 r_0/\tan\alpha$$

Hence the actual volume between the cones from r to r_0 is given by:

$$V_c = \pi\tan\alpha/3[3(r_0)^2 d/\sin\alpha + 3r_0 d^2/(\sin\alpha)^2 + d^3/(\sin\alpha)^3] - \pi r^2 d/\cos\alpha - \pi r_0 d^2/\tan\alpha$$

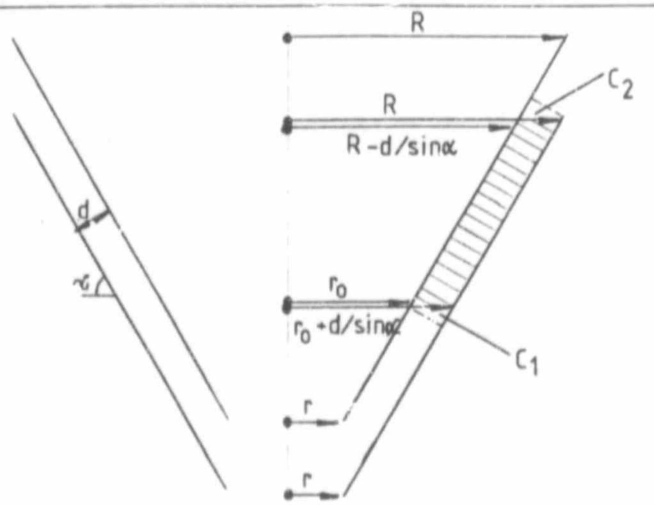

Figure 128. Dimensions of the laminar flow length.

Volume of a frustum of a cone:

$$V = \pi\tan\alpha/3((r_0)^3-r^3)$$

Substituting $r = r_0 + d/\sin\alpha$ and $r_0 = R$ for the outer cone gives:

$$V_1 = \pi\tan\alpha/3[\ R^3 - (r_0+d/\sin\alpha)^3\ ]$$

$$V_1 = \pi\tan\alpha/3[\ R^3 - (r_0)^3 - 3(r_0)^2d/\sin\alpha - 3r_0d^2/(\sin\alpha)^2 - d^3/(\sin\alpha)^3\ ]$$

Substituting $r_0 = R-d/\sin\alpha$ and $r = r_1$ for the inner cone gives:

$$V_2 = \pi\tan\alpha/3[\ (R-d/\sin\alpha)^3 - (r_0)^3\ ]$$

$$V_2 = \pi\tan\alpha/3[\{\ R^2 - 2Rd/\sin\alpha + d^2/(\sin\alpha)^2\ \}.\{\ R - d/\sin\alpha\ \} - (r_0)^3\ ]$$

$$V_2 = \pi\tan\alpha/3[\ R^3 - 2R^2d/\sin\alpha + Rd^2/(\sin\alpha)^2 - R^2d/\sin\alpha$$

$$+ 2Rd^2/(\sin\alpha)^2 - d^3/(\sin\alpha)^3 - (r_0)^3]$$

$$V_2 = \pi\tan\alpha/3[R^3 - 3R^2d/\sin\alpha + 3Rd^2/(\sin\alpha)^2 - d^3/(\sin\alpha)^3 - (r_0)^3]$$

Then volume of shaded area in the above figure:

$$V_T = V_1 - V_2$$

$$= \pi\tan\alpha/3[R^3 - (r_0)^3 - 3(r_0)^2d/\sin\alpha - 3r_0d^2/(\sin\alpha)^2 - d^3/(\sin\alpha)^3 - R^3 + 3R^2d/\sin\alpha - 3Rd^2/(\sin\alpha)^2 + d^3/(\sin\alpha)^3 + (r_0)^3]$$

$$V_T = \pi\tan\alpha[R^2d/\sin\alpha - Rd^2/(\sin\alpha)^2 - r_0d^2/(\sin\alpha)^2 - (r_0)^2d/\sin\alpha]$$

Volume of $C_1 = \pi d^2 r_0/\tan\alpha$

Volume of $C_2 = \pi d^2(R-d/\sin\alpha)/\tan\alpha$

Hence the actual volume between the cones from r_0 to R is:

$$V_c = V_T + C_1 + C_2$$

$$V_c = \pi\tan\alpha[R^2d/\sin\alpha - Rd^2/(\sin\alpha)^2 - r_0d^2/(\sin\alpha)^2 - (r_0)^2d/\sin\alpha] + \pi d^2 r_0/\tan\alpha + \pi d^2(R-d/\sin\alpha)/\tan\alpha$$

Nakamura model.

VOLUME AA'BB'. (See Chapter 7.2 for details).

$$V = \pi\tan\alpha[R^2d/\sin\alpha - Rd^2/(\sin\alpha)^2 - r_0d^2/(\sin\alpha)^2 - (r_0)^2d/\sin\alpha]$$

Where $R = r_0 + d/\sin\alpha$

and $r_0 = r_0 - (dk)/\tan\alpha$

$$V = \pi\tan\alpha[\ (r_0+d/\sin\alpha)^2 d/\sin\alpha - (r_0+d/\sin\alpha)d^2/(\sin\alpha)^2$$
$$- (d^2/(\sin\alpha)^2).(r_0-(dk)/\tan\alpha) - (r_0-(dk)/\tan\alpha)^2.d/\sin\alpha\ ]$$

$$V = \pi\tan\alpha[\ \{(r_0)^2 + 2r_0 d/\sin\alpha + d^2/(\sin\alpha)^2\}.d/\sin\alpha$$
$$- d^2 r_0/(\sin\alpha)^2 - d^3/(\sin\alpha)^3 - d^2 r_0/(\sin\alpha)^2$$
$$+ d^2(dk)/((\sin\alpha)^2\tan\alpha) + \{-(r_0)^2 + 2r_0(dk)/\tan\alpha$$
$$- (dk)^2/(\tan\alpha)^2\}\ ]$$

$$V = \pi[\ d^2(dk)/(\sin\alpha)^2 + 2r_0(dk)d/\sin\alpha - d(dk)^2/(\sin\alpha\tan\alpha)\ ]$$

Assuming that second order differentials are negligible, ie. $dk >> (dk)^2$, gives:

$$V = (dk).(\pi d^2/(\sin\alpha)^2 + 2\pi r_0 d/\sin\alpha)$$

VOLUME CEFGBA = ABGFH + HFEC.

For volume ABGFH:

$$V = \pi\tan\alpha[\ R^2 d/\sin\alpha - Rd^2/(\sin\alpha)^2 - r_c d^2/(\sin\alpha)^2$$
$$- (r_0)^2 d/\sin\alpha\ ]$$

Where $R = r_0 + d/\sin\alpha$
and $r_0 = r_0 - v(dt)/\tan\alpha$

$$V = \pi[\ d^2(v(dt))/(\sin\alpha)^2 + 2r_0(v(dt))d/\sin\alpha - d(v(dt))^2/(\sin\alpha\tan\alpha)\ ]$$

Volume HFEC:

$$V = \pi\tan\alpha/3[\ 3(r_0)^2 d/\sin\alpha + 3r_0 d^2/(\sin\alpha)^2 + d^3/(\sin\alpha)^3\ ]$$
$$- \pi r^2(v(dt))$$

Where $r_0 = r_0 - v(dt)/\tan\alpha$

and $r_0 = r_0 - (dk)/\tan\alpha$

$$V = \pi\tan\alpha[\ (r_0+d/\sin\alpha)^2 d/\sin\alpha - (r_0+d/\sin\alpha)d^2/(\sin\alpha)^2$$
$$- (d^2/(\sin\alpha)^2).(r_0-(dk)/\tan\alpha) - (r_0-(dk)/\tan\alpha)^2.d/\sin\alpha\ ]$$

$$V = \pi\tan\alpha[\ \{(r_0)^2 + 2r_0 d/\sin\alpha + d^2/(\sin\alpha)^2\}.d/\sin\alpha$$
$$- d^2 r_0/(\sin\alpha)^2 - d^3/(\sin\alpha)^3 - d^2 r_0/(\sin\alpha)^2$$
$$+ d^2(dk)/((\sin\alpha)^2\tan\alpha) + \{-(r_0)^2 + 2r_0(dk)/\tan\alpha$$
$$- (dk)^2/(\tan\alpha)^2\}\ ]$$

$$V = \pi[\ d^2(dk)/(\sin\alpha)^2 + 2r_0(dk)d/\sin\alpha - d(dk)^2/(\sin\alpha\tan\alpha)\ ]$$

Assuming that second order differentials are negligible, ie. $dk >> (dk)^2$, gives:

$$V = (dk).(\pi d^2/(\sin\alpha)^2 + 2\pi r_0 d/\sin\alpha)$$

VOLUME CEFGBA = ABGFH + HFEC.

For volume ABGFK:

$$V = \pi\tan\alpha[\ R^2 d/\sin\alpha - Rd^2/(\sin\alpha)^2 - r_0 d^2/(\sin\alpha)^2$$
$$- (r_0)^2 d/\sin\alpha\ ]$$

Where $R = r_0 + d/\sin\alpha$
and $r_0 = r_0 - v(dt)/\tan\alpha$

$$V = \pi[\ d^2(v(dt))/(\sin\alpha)^2 + 2r_0(v(dt))d/\sin\alpha - d(v(dt))^2/(\sin\alpha\tan\alpha)\ ]$$

Volume HFEC:

$$V = \pi\tan\alpha/3[\ 3(r_0)^2 d/\sin\alpha + 3r_0 d^2/(\sin\alpha)^2 + d^3/(\sin\alpha)^3\ ]$$
$$- \pi r^2(v(dt))$$

Where $r_0 = r_0 - v(dt)/\tan\alpha$